

UNIVERSITY OF ALGARVE
DEPARTMENT OF ELECTRICAL ENGINEERING AND COMPUTER SCIENCE
SIGNAL PROCESSING LABORATORY

ARRIVAL-BASED EQUALIZER FOR UNDERWATER
COMMUNICATION SYSTEMS

SALMAN IJAZ SIDDIQUI

UNIVERSITY OF ALGARVE, FARO

JANUARY 2012

UNIVERSITY OF ALGARVE
FACULTY OF SCIENCE AND TECHNOLOGY

ARRIVAL-BASED EQUALIZER FOR UNDERWATER
COMMUNICATION SYSTEMS

Salman Ijaz Siddiqui

Supervisor:

Prof. António João Freitas Gomes da Silva

DEPARTMENT OF ELECTRICAL ENGINEERING AND COMPUTER SCIENCE
SIGNAL PROCESSING LABORATORY

MASTERS IN ELECTRONICS AND TELECOMMUNICATIONS ENGINEERING

JANUARY 2012

Acknowledgements

It is my pleasure to thank all the crew of SiPLAB, which includes Dr. Sérgio M. Jesus, Dr. Orlando Rodríguez, Paulo Santos, Dr. António João Silva, Dr. Usa Vilaipornsawai, Néelson Martins, Dr. Paulo Felisberto, Dr. Cristiano Soares and Fred Zabel, for their support and useful advices throughout my work. SiPLAB is one of the well developed labs in Europe in underwater systems with the people working in underwater communications, ocean modeling, and development of underwater transmission and reception systems. It was a great pleasure to be part of such a diverse group which helped me a great deal in learning about different aspects of the underwater systems. I would like to show my deepest gratitude to my supervisor Dr. António João Silva for his precious time and valuable ideas. It was an honor for me to work under his supervision. I would like to acknowledge the support and guidance of Dr. Sérgio M. Jesus and Dr. Paulo Felisberto which helped me a great deal throughout my work. I would also like to thank Dr. Orlando Rodríguez who provided great insight about channel modeling which proved to be very helpful throughout my work. I would also like to thanks all other colleagues and friends specially Dr. Usa Vilaipornsawai, Néelson Martins and Fabio Lopes who supported me through good and difficult times and without their support I would not have accomplished it. I would also like to express my gratitude to Portuguese foundation for Science and Technology (FCT) and Technological Research Center of Algarve (CINTAL) for the financial support throughout the work. Finally, I would like to thank my beloved parents for their prayers and the moral support during the whole period of my study.

The work presented in chapter 2 was supported by Portuguese Foundation for Science Technology under UAB (POCI/MAR/59008/2004) and PHITOM (PTDC/EEA-TEL/71263/2006) projects. This work was also supported by European Community's Sixth Framework Programme through the grant to the budget of the Integrated Infrastructure Initiative HYDRALAB III within the Transnational Access Activities, Contract no. 022441. The authors would like to thank the R/V Gunnerus master and crew, HYDRALAB III and SINTEF personnel for their support during UAB'07.

The work presented in chapter 3 was partially funded by FCT Portugal (ISR/IST plurianual funding) through the PIDDAC Program funds and project PHITOM (PTDC/EEATEL/71263/2006). The authors would like to thank project WEAM(PTDC/ENR/70452/2006) who are the partner of CALCOMM'10 Experiment, chief scientist Dr. Paulo Felisberto and the ship crew for their support during CALCOMM'10.

Abstract

One of the challenges in the present underwater acoustic communication systems is to combat the underwater channel effects which results in time and frequency spreading of the transmitted signal. The time spreading is caused by the multipath effect while the frequency spreading is due to the time variability of the channel. The main purpose of this work is to address these problems and propose a possible solution to minimize these effects and to improve the performance of the underwater communication system.

The passive Time Reversal (pTR) equalizer has been used in underwater communications because of its time focusing property which minimizes the time spreading effect of the underwater channel. In order to compensate for the frequency spreading effect, an improved version of pTR was proposed in the literature, called Frequency shift passive time reversal (FSpTR).

In order to understand the effects of geometric variations on the acoustic signals, a Doppler based analysis technique, called Time Windowed Doppler Spectrum (TWDS), is proposed in this work. The principle of TWDS is to analyze the temporal variations of the Doppler spectrum of different arrivals received at a hydrophone. The results show that each arrival is affected in a different manner by the same environmental variation.

In this dissertation, an arrival-based equalizer is proposed to compensate for the environmental variations on each arrival. Due to complex multipath structure of the underwater channel, the arrivals are merged into one another in time and it is very difficult to separate them. The beamforming technique is used, in this work, to separate different wavefronts on the basis of angle of arrival. The arrival-based equalizer compensates for the environmental variations on each arrival separately using the FSpTR equalizer. The proposed equalizer is tested with the real data and the results shows that the proposed approach outperforms the conventional FSpTR equalizer and provides a mean MSE gain up to 3.5 dB.

Keywords: Underwater Communication, Passive Time Reversal equalizer, Frequency shift passive time reversal equalizer, Geometric variations, Beamforming

Resumo

Um dos desafios nos atuais sistemas de comunicação acústica submarina é o combate dos efeitos do canal submarino, os quais resultam no espalhamento temporal e frequencial do sinal transmitido. O espalhamento temporal é causado pelo efeito multicaminhos, enquanto o espalhamento frequencial é devido à variabilidade temporal do canal. O objetivo principal deste trabalho é abordar estes problemas, e propor uma solução para minimizar estes efeitos, para melhorar o desempenho do sistema de comunicação submarina.

O equalizador passivo Time Reversal (pTR) tem sido amplamente utilizado em comunicações submarinas, devido à sua propriedade de focagem temporal, o que minimiza o efeito de espalhamento temporal canal submarino. A fim de compensar o efeito de espalhamento frequencial, foi proposta na literatura uma versão melhorada do pTR, designada por Frequency shift passive time reversal (FSpTR).

A fim de compreender os efeitos das variações geométricas nos sinais acústicos, uma técnica de análise baseada em Doppler, designada por Time Windowed Doppler Spectrum (TWDS), é proposta neste trabalho. O princípio da TWDS é analisar as variações temporais do espectro Doppler de chegadas diferentes num determinado hidrofone. Os resultados mostram que cada chegada é afetada de uma maneira diferente pela mesma variação ambiental.

Nesta dissertação, é proposto um equalizador baseado nas chegadas, para compensar as variações ambientais em cada chegada. Devido à complexa estrutura multicaminhos do canal submarino, as chegadas apresentam-se fundidas no tempo, sendo muito difícil separá-las. A técnica de beamforming é utilizada, neste trabalho, para separar diferentes frentes de onda com base no ângulo de chegada. O equalizador baseado nas chegadas compensa as variações ambientais em cada chegada separadamente, usando o equalizador FSpTR. O equalizador proposto é testado com dados reais, e os resultados mostram que a abordagem proposta supera o equalizador FSpTR convencional, e apresenta um ganho médio em MSE de até 3.5 dB.

Palavras-chave: Comunicação Submarina, equalizador Passive Time Reversal, equalizador Frequency shift passive time reversal, Variações geométricas, Beamforming.

Contents

Acknowledgements	i
Abstract	iii
Resumo	v
1 Introduction	1
1.1 Underwater Channel Characteristics	4
1.2 Problem Formulation and Literature Review	8
1.2.1 Problem Formulation	8
1.2.2 Literature Review	9
1.3 Contributions	13
1.4 List of Publications	14
1.5 Organization of Dissertation	15
2 Passive Time Reversal and Geometric Variations	17
2.1 Introduction	17
2.2 Theoretical Background	19
2.2.1 Passive Time Reversal Communication System	20
2.2.2 Focusing Property of pTR Systems	21
2.2.3 Geometric Mismatch and FSpTR Compensation	23
2.3 Description of the UAB'07 experiment	25
2.4 Results and observations	28
2.5 Conclusion	30
3 Doppler decomposition of underwater acoustic channel	33
3.1 Introduction	33
3.2 Theoretical Background	35
3.3 Experimental description	39
3.4 Preliminary observations	41
3.5 Data processing and results	43
3.6 Conclusion	48
4 Beamformed FSpTR for underwater communications	51
4.1 Introduction	51
4.2 The beamformer with a vertical line array	53
4.3 The beamformer-FSpTR approach	57
4.4 The Beamformer-FSpTR communication system	62

4.5	Performance Comparison of FSpTR and BF-FSpTR	64
4.5.1	Simulated Data Scenarios	64
4.5.2	Simulated Data Results	67
4.5.3	Real data scenario	70
4.5.4	Real Data Results	71
4.6	Conclusion and Future Work	74
5	Conclusions	77

List of Figures

1.1	basic underwater scenario showing the source, receiver array of hydrophones and different paths from the source to the receiver	5
2.1	Probe and data signals underwater propagations (left); block diagram of FSpTR equalizer right: (i) filtering of hydrophone received data with time-reversed FS IR estimates, (ii) addition of filtered signals for each FS, (iii) selection of the FS signal with the maximum power, (iv) downsampling to the symbol rate and (v) estimate of the transmitted symbols	19
2.2	modeled source/array transect.	25
2.3	sound speed profile, CTD measured by the research vessel Gunnerus.	26
2.4	underwater channel characterization, a) arriving patterns estimated by pulse compression, b) Doppler spread of the channel during the 15 seconds, calculated at the 5 th hydrophone.	27
2.5	YOYO experiment: source depth variations over time. Start time is 12:40 pm.	27
2.6	FSpTR mean power as a function of time and frequency shift for 10 hydrophones (data set 1).	28
2.7	MSE comparison between FSpTR and pTR for 10 hydrophones with the source depth shift at 6 sec (data set 1).	28
2.8	FSpTR mean power as a function of time and frequency shift for 10 hydrophones.	29
2.9	MSE comparison between FSpTR and pTR for 10 hydrophones with the source depth shifts at 12 sec and 42 sec.	29
3.1	Two arriving paths from transmitter to the receiver, path p_1 is the direct path and path p_2 is the surface reflected path. V_T , V_R and V_S are the constant velocity vectors at the transmitting, receiving and the surface reflection point respectively. The unit vectors \hat{n}'_T and \hat{n}'_R represents the directions of the propagation of the transmitted and received signal for the direct path while \hat{n}''_T and \hat{n}''_R represents the unit vectors for the surface reflected path.	37
3.2	(a) downward refracting sound speed profile during Day 2 (b) Day 2 bathymetry map of the work area with GPS estimated locations of AOB21 and AOB22 deployments and their recovery, ship/source track (dotted lines) and ship track during communication events (green lines).	40
3.3	IR estimates: (a) for 16 hydrophone array and white lines showing the selected wavefront (b) the temporal evolution of IR along 15 sec of transmission for channel 3.	40
3.4	ray tracing diagram of the signal propagation over the environment of CAL-COMM'10	42

3.5	(a) variability of the selected wavefront shown in figure 3.3 (a), (b) corresponding Doppler spread of the selected wavefront	43
3.6	(a) Doppler computed only for 4 sec time window, centered at 4.5 sec, where two lobes can be seen; the first due to one main arrival at ~ 0.01 Hz and the second due to the surface reflected arrival at approximately 0.5 Hz (b) Doppler summation along the delay axis	45
3.7	(a) Doppler computed only for 4 sec time window, centered at 5.5 sec, where three lobes can be seen; the first due to the main arrival at ~ 0.1 Hz and the other two due to the surface reflected arrival at ~ -0.4 Hz and ~ 0.5 Hz (b) Doppler summation along the delay axis	45
3.8	(a) Doppler computed only for 4 sec time window, centered at 6.5 sec, where two lobes can be seen; the first due to the main arrival at ~ 0.1 Hz and the second due to the surface reflected arrival at ~ -0.4 Hz (b) Doppler summation along the delay axis	45
3.9	(a) summation along the delay axis of Doppler-delay diagram computed by only TWDS analysis (b) summation along the delay axis of Doppler-delay diagram computed by combination of TWDS and WT.	47
4.1	basic underwater scenario showing the source, the receiver and different arrivals from the source to the receiver. The VLA beamformer is implemented on the receiver to isolate different arrivals depending on the angle of arrival, by steering the beams along the water column.	54
4.2	Plane Wavefront arriving at each element of the array with different delays	55
4.3	Time and Frequency Domain Implementations of the beamformer	55
4.4	simulated channel characterization: a) channel IR estimates b) the beamforming result showing the angle of arrival of different arrivals taking hydrophone 8 as the reference hydrophone, so the delay axis is representing the delay for each wavefront w.r.t hydrophone 8.	56
4.5	Block Diagram of the BF-FSpTR	58
4.6	(a) Output of the combining block in figure 4.5 considering no frequency shift and identical IRs: (a) angle delay-spread plane, (b) sum over the angles, z_{output}	60
4.7	(a) Output of the combining block in figure 4.5 with no frequency shift and using mismatched IRs: (a) angle delay-spread plane, (b) sum over the angles, z_{output}	60
4.8	(a) Output of the combining block in figure 4.5 with optimal frequency shift compensation and using mismatched IRs: (a) angle delay-spread plane, (b) sum over the angles, z_{output}	60
4.9	block diagram of the BF-FSpTR system, applied to underwater communications	62
4.10	downward refracting sound speed profile.	64
4.11	Doppler spread, at hydrophone 6 placed at 26 m depth, due to a source vertical motion of 0.5 m/s.	65
4.12	Doppler spread, at hydrophone 6 placed at 26 m depth, due to a source vertical and horizontal motion of 0.5 m/s each	66
4.13	case (i) MSE performance of FSpTR and BF-FSpTR with a beamformer angular range of of -10 to +10 degrees.	68
4.14	case (i) MSE performance of FSpTR and BF-FSpTR with a beamformer angular range of of -50 to +50 degrees.	68

4.15 case (ii) MSE performance of FSpTR and BF-FSpTR with a beamformer angular range of of -50 to +50 degrees.	69
4.16 channel IR estimates of the real dataset.	70
4.17 The Beamforming result showing the angle of arrival of different arrivals . . .	71
4.18 real data MSE performance comparison between FSpTR and BF-FSpTR with a beamformer angular range of of -10 to +10 degrees	72
4.19 real data MSE performance comparison between FSpTR and BF-FSpTR with a beamformer angular range of of -50 to +50 degrees	72

List of Tables

3.1	Signal Specification for the CALCOMM'10 Experiment	41
-----	--	----

Chapter 1

Introduction

Underwater acoustic communication is a rapidly growing field of research due to rapid increase in the use of underwater application for commercial purposes. Some of the applications in which underwater communication is employed are monitoring of off-shore oil industries, collection of scientific data from the ocean-bottom stations and environmental surveying. With the current advancement in the underwater applications, the user requirements also increases in terms of system throughput and performance. In order to cope with these requirements, there is a need of robust underwater system which can adapt to the adverse underwater perturbations and also satisfies the user requirements of bandwidth efficiency and low cost.

In the past underwater communication was done through physical media e.g. underwater cables. Although underwater cables provide high bandwidth for communications, they are very vulnerable to adverse underwater conditions and requires frequent repairs. The cost of these repairs is very high. Moreover, a very skilled labor is required which further increases the cost, making it a very unsuitable solution.

In the current underwater acoustics communication systems, the transmission link is established by acoustic waves, which travel from the source to the receiver through the underwater

channel. These wireless underwater applications overcome the disadvantages of the physical media but offer a great deal of challenges due to limited bandwidth availability and several time-variant perturbations, e.g. source/receiver motion and surface waves variations. The acoustical link depends on the position of the source and the receiver relative to the non-uniform medium, i.e. a change in the source/receiver position causes a change in the received signal. In underwater environment, it is practically impossible to make the source and the receiver stationary and even when the source and the receiver are attached to the bottom, the surface and internal waves as well as tides cause the medium to vary. Due to these variations, the underwater acoustic channel changes strongly with time. In order to improve the performance of the communication systems, it is important to keep track of these variations. The main objectives of this work are to develop a technique for observing the effects of these variations on acoustic signals and to improve the performance of the current underwater equalizers by adapting them to these variations.

The underwater channel is a doubly spread channel which spreads both in time and frequency. During the transmission, the transmitted signal reaches the receiver through different paths and experiences different delays depending on the path length. These delayed replicas produces spreading in time in the received signal and this effect is called multipath effect. Due to long multipath spread of the underwater channels, the intersymbol interference (ISI) increases, affecting adversely the performance of the underwater communication system. In order to minimize the multipath effect, linear equalization methods [1, 2] and direct spread spectrum techniques [3, 4] are proposed in the literature. On the other hand, the frequency spreading is caused by the channel multipath variations, which among others are governed by the source/receiver motion and surface variations.

In the last decade Passive Time Reversal (pTR) communication emerged as an effective technique for underwater acoustic communications to combat ISI [5, 6, 7]. In pTR, a single source and a vertical line array (VLA) is used. A probe signal is transmitted ahead of the data for the channel IR estimation. The IR estimate is then used as a synthetic channel for the temporal focusing of the data signal, which is equivalent to the deconvolution of the multipath generated by the real channel. The performance of pTR degrades in the presence of geometric variations like source/receiver motion and surface variations which induce channel frequency-spread. An improved version of pTR called Frequency Shift Passive Time Reversal (FSpTR) equalizer is introduced in [8] to combat the effects of geometric variations. In FSpTR, a frequency shifted version of the IR estimate are correlated with the received data and the optimal frequency shift is selected based on the maximum output power. The main difference between FSpTR and pTR is that in FSpTR the channel IR is frequency shifted before correlating with the received signal while in pTR the channel IR is directly correlated with the received signal. It has been shown in [8] that FSpTR can track the geometric variations by applying an appropriate frequency shift which improves the performance of the communication system.

In the real environment at a sufficient distance from the source, the channel multipaths arrive to a VLA in wavefronts reaching the receiver from different angles, where each wavefront is a combination of a group of modes [8] in the normal mode model context. In order to achieve the maximum performance gain of the FSpTR, each group of modes must be compensated independently for the environmental effects, by applying an appropriate frequency shift. The main problem in doing so is that all the wavefronts in the received IRs are merged with one another and it is not possible to identify and separate them.

One of the contributions of this work is to analyze the effects of the environmental variations on each arrival in the multipath environment using Doppler-based analysis and observe these variations along time to understand the time variability of the underwater channel. Such analysis suggests that the performance of the FSpTR system can be improved by isolating different channel wavefronts and compensating for each wavefront-variability separately. Beamforming (BF) applied with a VLA is a technique that allows to separate different arriving wavefronts and will be used in this work.

Another contribution of this work is a technique, called Beamformed-FSpTR (BF-FSpTR), which combines BF with FSpTR. The main principle of the BF-FSpTR is to integrate beamformer with FSpTR, by using the beamformer to isolate different wavefronts based on the angle of arrival which are then fed to FSpTR separately. Since each wavefront is affected by different environmental variations, FSpTR applies different frequency shift to each path to compensate for the time-variable effects. The resulting compensated wavefronts are then summed up to give the output of BF-FSpTR.

1.1 Underwater Channel Characteristics

Underwater channel can be categorized as an acoustic waveguide which is bounded from above by the sea surface and from below by the sea floor. Figure 1.1 shows the basic underwater scenario where the wave propagation depends on two spatial variables, range ' r ' and depth ' z '. Any arbitrary location in the scenario can be represented by location ' (r, z) ' in the range-depth plane. In figure 1.1, the source location is considered to be the point of reference which is $(0, z_s)$, and the hydrophone array is located at the distance r_0 from the source. Thus

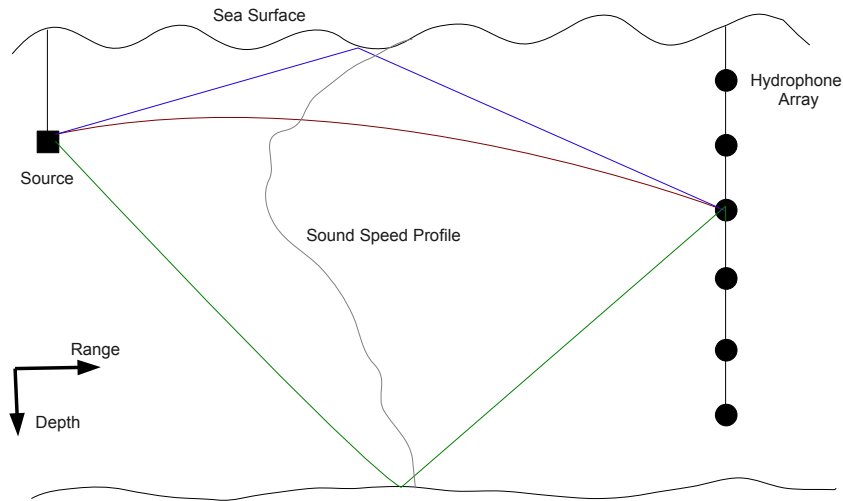


Figure 1.1: basic underwater scenario showing the source, receiver array of hydrophones and different paths from the source to the receiver

the location of each hydrophone in the array becomes $(r_0, z_1), (r_0, z_2), \dots, (r_0, z_I)$ where I is the number of hydrophones in the array. The grey line across the water column is the sound speed profile. The sound speed profile is a function of temperature, salinity and pressure and varies with the water column depth. It defines the behavior of the sound propagation in the underwater medium. The attenuation experienced by sound depends on the distance traveled, and on the number of reflections on the bottom and on the surface.

In figure 1.1, different arrivals are shown from the source to the array. The direct arrival (shown in red color) is the one without any surface or bottom interaction so it is only affected by the source and array movement and sound speed profile variations. The surface reflected arrival (shown in purple) is also affected by surface variations in addition to the above mentioned variations. The bottom reflected arrival (shown in green) is mainly affected by the bottom properties which are specified as density, compressional speed and attenuation. This is a simplified diagram showing only the single reflected arrivals while in real environment there are several other arrivals which reach the receiver after many surface and

bottom reflections.

The sound propagation in the underwater channel, due to a point source, is usually modeled with the help of different propagation models; namely the fast field program (FFP), normal mode (NM), ray tracing, parabolic equation (PE) models. In this work, normal mode and ray tracing models are considered because the (principle of) pTR can be explained (in chapter 2) with the help of normal mode model, while the effect of environmental variations on each arriving path can be better explained by ray tracing model (in chapter 3).

In normal-mode solutions, the acoustic energy is considered to be a weighed sum of normal modes [9]. The normal mode approach reduces the complexity of the range independent environment, since there is no need to calculate the mode function at all the intermediate ranges between the source and the receiver [10]. On the other hand in case of a range-dependent environment, which may be due to range variations of the sound speed profile or of the boundary conditions, the normal mode solution becomes more complex.

The ray tracing approach is a pictorial representation of the acoustic field in the form of a ray diagram. From the ray diagram it is easy to identify different arrivals and it is also possible to find the delay in each arrival which is directly proportional to the length of the ray. With the ray tracing model, it is difficult to handle the wave effects like diffraction. [11].

The ray tracing model is based on the principle of optics and the basic assumption in the model is that the wavelength of operation must be smaller than the geometric dimensions of the objects in the propagation environment. This assumption is termed as "high frequency approximation" and it compromises the accuracy of the model results [12]. On the other hand, it provides better results in range-dependent environments where the rays can be

traced through range-dependent sound speed profiles and over complicated bathymetry[13]. In both the normal mode and the ray tracing models, the channel is modeled as time invariant which means that the channel remains static during a single transmission time period. However, in the real environment the underwater channel is time-variant and spreads both in delay and Doppler [14].

In an underwater communication system, multipath propagation causes intersymbol interference (ISI), which results in spreading of the received signal. The knowledge of the multipath propagation geometry plays a vital role in suppressing the multipath effects. The recent developments in propagation models have made them capable of predicting the multipath configuration. In [15, 16], ray tracing is used for determining the multipath structure for communication channel modeling.

All the environmental effects, e.g surface waves variations, source/receiver motion etc, contribute in the time variability of the underwater channel. Due to this time variable behavior, the received signal spreads in the frequency domain and this phenomenon is termed as Doppler spread. The Doppler spread is dependent on the operating frequency. In short range applications (below 100 m) high frequencies are used, the Doppler spread is high. On the other hand, for long range applications (between 1-10 km) where lower frequencies are used, the Doppler spread is relatively low. In order to model the Doppler spread of the time-variable acoustic channel, a Time Variable Acoustic Propagation Model (TV-APM) was proposed in [17] which simulates the Doppler distortion in the received signals and is useful in analyzing the performance of equalizers for underwater communication systems.

1.2 Problem Formulation and Literature Review

The main problems in underwater communication systems are to predict and compensate for the changes in the underwater channel and to minimize the effects of these changes on the communications systems. These changes can be categorized as the intrinsic changes and extrinsic changes. The intrinsic changes include the temperature changes in different layers of the underwater channel, the surface motion and internal waves. These changes are categorized as intrinsic because they can not be controlled. On the other hand, the movement in the source and the receiver is considered as the extrinsic changes, because they can be tracked and controlled. In order to improve the performance of the underwater communication system, it is necessary to minimize the effects of these changes. The objectives of this work are to track these changes, study their effects and define strategies to reduce their influence in underwater communication systems with time-variable channels.

1.2.1 Problem Formulation

In the ocean acoustic channel, strong amplitude and phase fluctuations occur during acoustic transmissions. Sources of these fluctuations can be the internal waves, turbulence, temperature gradients and other related phenomenon which result in variations in the sound speed profile. These perturbations interact with the acoustic wavefronts that arrive to the VLA of hydrophones, producing refractive and diffractive effects at the VLA. These effects cause the temporal, spatial and frequency-dependent fluctuations in the received waveforms. In addition to these effects, there are multiple propagation paths between transmitter and receiver and the time-variant interference between these paths also results in fluctuations in the received signal power [18].

In correlation based equalizers like pTR, a transmitting source and a VLA of receivers are considered. The received data is correlated with previously estimated channel impulse responses (IRs). The pTR system compensates for the multipath effects by providing focusing in the time domain [19]. In addition to single carrier systems, the pTR technique is also tested with multicarrier systems, e.g. OFDM modulated signal, in order to attain higher data rates and to combat frequency selective fading channels [20, 21]. The performance of pTR systems degrades in the presence of geometric variations which produce mismatch between the initial channel IR estimates and the channel IRs during data transmission, thus resulting in imperfect time domain focusing.

A possible solution for combating the geometric variations was proposed in [8] where the IR mismatch is compensated by applying different frequency shifts to the estimated IRs in the pTR processing. This scheme works well in case of a well-separated arrival structure where each arrival can be separated by applying a time window. However, this is not always the case in practice, as different arrivals reach the receiver very closely spaced in time or overlap on each other. In this case, the Frequency Shift Passive Time Reversal (FSpTR) is unable to give the desired result. In this work, a more robust version of FSpTR is proposed which uses a beamformer to distinguish different arrivals, making it possible to apply different frequency shifts to each arrival, and each arrival is used individually to maximize the performance of the system.

1.2.2 Literature Review

The work presented in this dissertation addresses two different issues in underwater communication systems. The first one is to study the effects of environmental variations on

the communication signals and secondly to use this analysis to improve the performance of the current underwater communication system. This section will provide a literature review of both of these topics. The first part of this section will address the current underwater communication systems and the equalization techniques while the second part will elaborate the techniques used to study the effects of environmental variations.

Due to the recent developments in underwater acoustic systems, there is a growing interest in deploying different modulation schemes and equalizers for different applications e.g. remote sensing, speech and image processing and telemetry. Both coherent and non-coherent modulation schemes are employed in current underwater systems depending on the application. In this work, a coherent modulation scheme is used. Hence, in this section, the emphasis is given on coherent modulation schemes for underwater communication systems [22].

The main problem in employing coherent modulation schemes is that it is very difficult to retrieve the reference carrier frequency (keeping in mind the complex multipath structure of the underwater channel). This problem was addressed in [23]. Different equalization methods are employed to combat multipath effects. In [1, 2], Differential Phase shift Keying (DPSK) is used with linear equalization, while in [3, 4] direct sequence spread spectrum techniques are employed in underwater communications systems.

The performance of the underwater channel equalizers can also be enhanced by exploiting spatial diversity techniques which help in combating ISI due to multipath propagation [24]. In [25], Stojanovic proposed the Channel Estimate based Decision Feedback Equalizer which used multichannel combining with the equalization technique to exploit the spatial gain as well as the equalization gain. By employing these techniques, the performance is greatly improved but it is at the cost of a high computation at the receiver. The complexity of

the system can be reduced by using spatio-temporal multichannel equalizers [26]. Another approach is to use retrofocusing techniques which reduce the complexity of the system by splitting the computational complexity between the transmitter and the receiver [27]. The simplest case of retrofocusing is the Time Reversal Communication system (which is phase conjugation in the frequency domain) [28].

The Time Reversal communication system offers lower complexity than traditional equalization systems and the spatial and temporal focusing capability of time reversal systems makes it most favorable for communication applications specially in a multipath environment [29, 30, 31]. In time reversal communication, as discussed earlier, the received signal is correlated with the time reversed version of the estimated impulse response of the channel. There are two types of time reversal systems namely active time reversal (aTR) and passive time reversal (pTR). The main difference between aTR and pTR is the direction of flow information. In the active case, the information can be sent from the array back to the distant source, while in passive case only the source sends the information to the receiver. The main assumption in time reversal systems is the time reciprocity principle, which means that the channel remains unchanged during the transmission from the transmitter to the receiver and the retransmission from receiver to the transmitter [6]. This property allows to retransmit a time-reversed version of a multipath dispersed probe pulse back to its origin, where the probe signal contains the multipath structure of the channel. This process is analogous to considering the ocean as a matched filter in which the transfer function of the medium is embedded in the probe signals. The aTR system takes the advantage of reciprocity principle and matches the ocean response with itself while the pTR system uses the estimated channel IR to perform a virtual ocean response match [8].

The main problem with the passive time reversal communication system is that it fails in case of environmental variations like source/receiver geometric variations and/or underwater channel variations. In [14], Preisig compared the performance of channel estimate based decision feedback equalizer (CE-DFE) [32] and pTR equalizer in the presence of imperfect channel estimates. The results suggested that the performance of these equalizers degrades significantly in the presence of rapid environmental variations, e.g. sea surface variations. In [14], a robust CE-DFE was also proposed to mitigate the effects of these channel variations. The results of robust CE-DFE showed that it provides the performance improvement but can not eliminate the effects completely.

In order to compensate for the source and receiver movement, an improved version of pTR is proposed in [8], called Frequency Shift Passive Time Reversal (FSpTR) system. FSpTR equalizer was designed to compensate for the source/receiver variations by applying appropriate frequency shifts. In [33] DFE was integrated with FSpTR to mitigate the residual ISI and further improve the performance of the FSpTR communication system.

The performance of the time reversal system degrades significantly in the presence of environmental variations. This work proposes a technique to analyze the effect of these variations on acoustic signals. Different techniques have been proposed in the literature to understand the effects of environmental variations on acoustic signals. IR estimation is one of the most simple and effective techniques used to estimate different geometric variations [34]. To estimate the IR, different matched filtering techniques are employed where the received signal is correlated with the time delayed versions of the transmitted signal. The idea of using matched field processing is to find the mismatch between the transmitted signal and the received signal which gives the information about the environmental variations. In [35] Delay-Doppler

Spread functions (DDSF) are proposed for characterizing different environmental variations. DDSF are obtained by computing the instantaneous IR as a function of delay and time and then taking the Fourier transform along the time variable. DDSF helps in estimating the geometric information like source/receiver position and motion[36, 37]. The main drawback of DDSF is its computational complexity. In order to address this problem low complexity algorithms based on matching pursuit (MP) and orthogonal matching pursuit (OMP) are used to compute the DDSF coefficients [38]. In [39], an alternative basis pursuit method was proposed for estimating the DDSF coefficients which further reduces the computational complexity. The efficiency of this method was also presented by comparing the results with the predictions of the ray propagation model.

In recent literature, different Doppler-based analysis techniques are proposed for tracking environmental variations. In [40], two simulation methods are described for modeling time varying sea surface using ray theory and ray based formulation of the Helmholtz integral equation with a time domain Kirchoff approximation. In [41], a matched filtering technique is used to estimate IR and to study the effect of environmental variations caused by source/array movement and sea surface motion on the impulse response. In both [40] and [41], the Doppler shifted replicas of the transmitted signals are matched filtered with the received signal and depending on the peak in the ambiguity plane, source/receiver motion and surface variations are estimated.

1.3 Contributions

The contributions of the dissertation can be summarized as follows:

1. The FSpTR is applied on the real data of UAB'07 experiment and source depth changes are successfully detected and compensated by the equalizer (Chapter 2).
2. A Doppler-based scheme called Time Windowed Doppler Spectrum (TWDS) is proposed which can be used to analyze the temporal evolution of different environmental variations. The main idea of TWDS is to observe the temporal variations in the IR by analyzing it in small time windows instead of the whole signal at a time. This helps in analyzing the effects of environmental variations on each path separately. By doing so, it is possible to differentiate between different paths arriving from the transmitter to the receiver. In this work, TWDS is used to detect the surface waves motion (Chapter 3).
3. An improved version of FSpTR is proposed based on the observations of TWDS, called Beamformed FSpTR (BF-FSpTR). The principle of BF-FSpTR is that the beamformer is used to isolate each path from the transmitter to the receiver and these isolated paths are fed to the FSpTR equalizer. Since each path is affected by the environmental variations in a different manner, FSpTR compensates each path by selecting different frequency shifts(Chapter 4).

1.4 List of Publications

The following two conference papers are published during the course of this work

1. S. Ijaz, A. Silva and S. M. Jesus, "Compensating for Source Depth Change and Observing Surface Waves Using Underwater Communication Signals", *International Conference on Sensor Technologies and Applications (SENSORCOMM), Venice, Italy*. Pages

462-467, July, 2010

2. S. Ijaz, A. Silva, O. C. Rodríguez and S. M. Jesus, "Doppler domain decomposition of the underwater acoustic channel response", *OCEANS 2011 IEEE Conference, Santander, Spain*. pages 1–7, June 2011.

1.5 Organization of Dissertation

Chapter 2, 3 and 4 of the dissertation are written in the form of papers. The dissertation is organized as follows:

Chapter 2 will explain passive time reversal (pTR) and frequency shift passive time reversal communication (FSpTR) system in detail with some experimental results from the Underwater Acoustic Barrier 2007 (UAB'07) sea trial. In this experiment sudden depth changes of 0.5 m are performed intentionally to check the performance of FSpTR in case of source depth change.

Chapter 3 will elaborate some techniques used for tracking the environmental variations. A Doppler-based technique is proposed in this chapter for tracking the source/receiver motion and surface variations. Some results from the real data of CALCOM'10 experiment are also presented.

Chapter 4 will present a modified version of FSpTR which integrates the beamformer with the FSpTR. The main idea is to combine the FSpTR equalizer presented in chapter 2 with the observations about the environmental variations explained in chapter 3. Some results from the simulated data as well as real data are presented in this chapter to show the effectiveness of the scheme.

Chapter 5 will give the conclusion of the dissertation and future work.

Chapter 2

Passive Time Reversal and Geometric Variations

2.1 Introduction

One of the most active research topics nowadays is to design effective signal processing techniques for underwater communications. This interest is magnified by the challenges due to uncontrollable conditions such as temperature, bottom bathymetry and geometric changes like source and array depth variations. The attainability of even modest data rates is still a challenge due to these variations. In recent research literature many channel estimate based equalizers have been proposed to cope with these changes [32, 19, 42]. Channel estimate based equalizers are those for which observations of the received signal are used to estimate the channel impulse response and possibly the statistics of interfering noise. One of the example of channel estimate based equalizer is the passive Time Reversal (pTR) equalizer [5, 6, 7]. In pTR, a receive only array is used and a probe-signal is transmitted ahead of the data for channel Impulse Response (IR) estimation. The IR estimate is then used as a synthetic channel that after cross-correlation with the IRs, results in the temporal focusing of the data signal, which is equivalent to the deconvolution of the multipath generated by the real channel.

In correlation-based equalizers like pTR, source and array depth shifts are the major bottlenecks due to continuous amplitude and phase changes in the IR. In order to address this problem many solutions have been proposed, which include (i) to transmit a probe signal more frequently (ii) to use an adaptive algorithm to track the IR from the initial probe signal IR estimation [42], (iii) to use a low complexity equalizer with only one coefficient per channel [43] and (iv) Frequency Shift Passive Time Reversal (FSpTR) that is an environment-based equalizer which attempts to compensate for the Doppler shifts due to the environmental variations[8].

In this chapter, an environment based pTR equalizer is used, which is based on waveguide invariant properties of the underwater channel [44]. It was found that by using these waveguide invariants, geometric changes such as source and array depth can be compensated by applying an appropriate frequency shift on the IR estimates, which are obtained during probe signal transmission. By doing so the output power of the Frequency Shift pTR (FSpTR) equalizer will increase resulting in lower Mean Square Error (MSE) [12].

In this chapter, real data collected from UAB'07 sea trial was processed. The UAB'07 experiment was performed during the first two weeks of September 2007 in Trondheim, Norway. The communication experiment conducted during UAB'07 aimed at testing the performance of the FSpTR. During the sea trial sudden changes of 0.5 m were made in the source depth at various known instants of time. The results show that FSpTR successfully tracked these changes and applied appropriate frequency shift in the IR to compensate for these changes resulting in a gain in MSE and bit error rate (BER).

The chapter is organized as follows: Section 1 presents a detailed theoretical background of pTR in a stationary environment, the performance losses of pTR in cases of source and

array depth changes and illustrates how the frequency shift compensates for these changes, Section 2 provides a description of the UAB'07 experiment and steps of data processing and section 3 elaborates the results obtained by the FSpTR equalizer, Section 4 concludes the chapter with a brief summary and future work.

2.2 Theoretical Background

A passive time reversal communication system is a point to multi point system consisting of a source and a vertical line array (VLA). The procedure begins with the transmission of a single probe pulse from a distant source and the reception of the response at each element of the array. The signal processing steps involves cross correlating the received probe signal with the data stream received at each element of the VLA. This cross correlation is done in parallel at each array element and the results are summed across the array to get the final output signal. It is assumed, with no loss of generality, that the transmitted probe signal will be a Dirac pulse. The theoretical background presented here follows ref. [6, 8].

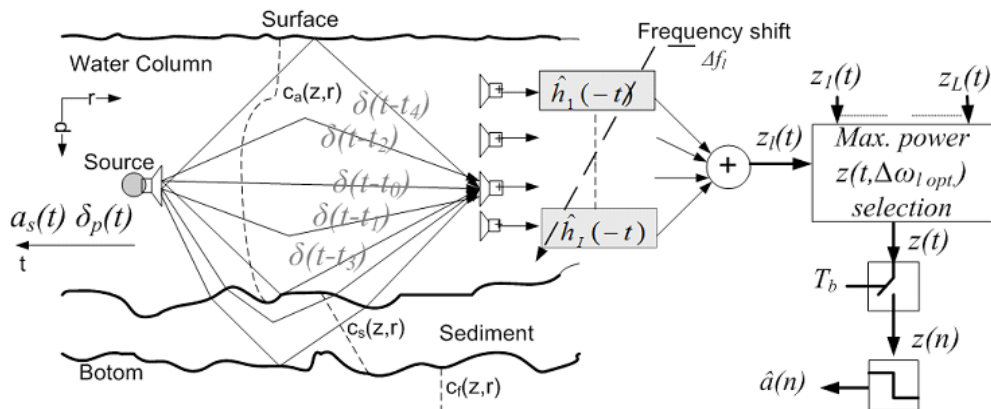


Figure 2.1: Probe and data signals underwater propagations (left); block diagram of FSpTR equalizer right: (i) filtering of hydrophone received data with time-reversed FS IR estimates, (ii) addition of filtered signals for each FS, (iii) selection of the FS signal with the maximum power, (iv) downsampling to the symbol rate and (v) estimate of the transmitted symbols

2.2.1 Passive Time Reversal Communication System

Figure 2.1 shows the basic geometry of the underwater FSpTR communication system. The source transmits the probe signal $\delta_p(t)$ which reaches the array through several paths. Assuming all the paths are cleared, then the data stream $a_s(t)$ is transmitted. Due to dispersion and multipath effect the probe signal expands in time domain. Similarly the data signal is also broadened resulting in intersymbol interference (ISI) due to temporal overlap. As shown in the figure, each element of the VLA receives the signal through different paths thus each received signal is affected by different dynamics of the environment. At each element of the VLA the received data stream is cross-correlated with the received pulse signal.

$$y_i(t) = (\delta(t) * a(t)) * (h_i(t) * h_i'^*(-t)) \quad (2.1)$$

where i is the hydrophone index, $h_i'(t)$ is the channel IRs during probe transmission and $h_i(t)$ is the channel IRs during the data transmission which is affected by the channel variations resulting in a mismatch between h_i and h_i' . The output of the cross-correlator along each element $y_i(t)$ is summed to get the output signal $z(t)$.

$$z(t) = \sum_{i=1}^I y_i(t) \quad (2.2)$$

The right part of the block diagram shows the frequency shift processing. During the process, a frequency shift $\Delta\omega_l$ is applied to the estimated channel IR during probe transmission $h_i(t)$ so the output of the cross correlator $y_i(t, \Delta\omega_l)$ across each hydrophone, becomes

$$y_i(t, \Delta\omega_l) = (\delta(t) * a(t)) * (h_i(t, \Delta\omega_l) * h_i'^*(-t)) \quad (2.3)$$

where $l = [1, 2, \dots, L]$ denotes the set of frequency shifts. The output $y_i(t, \Delta\omega_l)$ is summed over all elements of the array to get $z_l(t)$

$$z_l(t) = \sum_{i=1}^I y_i(t, \Delta\omega_l) \quad (2.4)$$

This $z_l(t)$ is fed to the maximum power selection block which selects the optimum frequency shift depending on the maximum received power.

2.2.2 Focusing Property of pTR Systems

The most attractive feature of pTR is its focusing property. During the transmission of the signals through the underwater channel, it is affected by numerous channel variations. The main idea of exploiting the focusing property of the pTR system is to minimize the effects of these perturbations to improve the performance of the communication system.

The focusing in time is achieved by match filtering the IR from the source to the i^{th} hydrophone of the array and summing it over all hydrophones. The main advantages of this operation is that the time elongation due to multipath propagation is reduced[45]. The back propagation and summing operation over all hydrophones is a form of spatial matched filtering which improves the temporal focusing by suppressing the side lobes. The focusing operation of pTR can be expressed in a mathematical form using normal modes approach. Using the normal mode model the acoustic field generated by a monochromatic point source in a perfect waveguide at the i^{th} element of the VLA is given by the Green's function [12]

$$G_\omega(R, z_0, z_i, \omega) = \frac{-j}{\rho\sqrt{8\pi R}} e^{\frac{-j\pi}{4}} \sum_{m=1}^M \frac{Z_m(z_i)Z_m(z_0)}{\sqrt{k_m}} e^{-jk_m R} \quad (2.5)$$

where m is the mode number, M is the total number of propagating modes, ρ is the water column density, R is the source-array range, $Z_m(\cdot)$ is the m^{th} mode shape, z_0 is the source

depth, z_i is the depth of the i^{th} element of the VLA and k_m is the m^{th} mode horizontal wavenumber. Considering (2.1) and (2.2), the resulting synthetic impulse response (IR) is the sum of the convolutions between the channel IRs during probe transmission and channel IRs during data transmission. In frequency domain, the synthetic pTR IR acoustic field in a stationary environment is given by

$$P_{pc}(R, z_0, z_i, \omega) = \sum_{i=1}^I G_\omega(R, z_0, z_i) G_\omega^*(R, z_0, z_i) \quad (2.6)$$

$$= \frac{1}{\rho^2 8\pi R} \sum_{m=1}^M \sum_{n=1}^N \frac{Z_m(z_0) Z_n(z_0)}{\sqrt{k_m k_n}} \Psi(m, n) e^{j(k_m R - k_n R)} \quad (2.7)$$

where $\Psi(m, n)$ is the product of mode shape functions, summed over all the elements of the array. Assuming that the array spans the entire water column and the elements of the array sample the water column sufficiently to fulfill the orthogonality property [19], the product of the mode shape function becomes

$$\Psi(m, n) = \sum_{i=1}^I Z_m(z_i) Z_n(z_i) \approx \delta_{m,n} \quad (2.8)$$

putting this value in equation (2.7) and after simplification the synthetic pTR acoustic field becomes

$$P_{pc}(R, z_0, z_i, \omega) = \frac{1}{\rho^2 8\pi R} \sum_{m=1}^M \frac{|Z_m(z_0)|^2}{|k_m|} \quad (2.9)$$

since equation (2.9) is weakly dependent on frequency, it results that in time domain we have a Dirac impulse.

Pulse compression is also an effective feature of the pTR systems. As shown above, the sum of the convolution of Green functions across each element of the VLA results in a Dirac impulse and by summing across the array the side lobes are suppressed. However, in case of mismatch between the Green functions, which can be due to source array range and depth variations, this Dirac is distorted which causes a loss in the performance of the system.

2.2.3 Geometric Mismatch and FSpTR Compensation

When pTR is applied in a stationary environment and the array samples the environment ideally, there is a complete match between the channel IR during probe signal transmission and channel IR during data transmission which result in a Dirac impulse in the time domain as seen in equation (2.9). But the environmental/geometric variations produces a mismatch between the channel IRs, which results in distortion of the Dirac impulse and also produces side lobes which results in the degradation of the performance of the pTR system. Several solutions have been suggested to combat this problem which involve transmitting the probe signal more frequently, using the adaptive algorithm to track the IR from the initial probe signal or using a single tap equalizer to track channel variations. The comparison of these techniques is presented in [43]. In [8] an environment-based equalizer, called FSpTR, was presented which is based on the waveguide invariant properties of the underwater channel. In [46] a relation is provided which relates the variation in range to the change in angular frequency

$$\frac{\Delta\omega}{\omega} = \beta \frac{\Delta r}{R} \quad (2.10)$$

where ω is the center frequency, R is the source array range and β is the horizontal waveguide invariant. In [44] the existence of β was firstly studied for the real environment. In [47], an appropriate frequency shift was applied in active time reversal to refocus at ranges other than that of the probe sources using β and in [48] the waveguide invariants were first applied to compensate for the source array range variability in the communication systems

The basic idea of FSpTR is to apply the waveguide invariant property to compensate for range mismatch by appropriately shifting the spectral components of the data used for the

time reversal operation. In the presence of geometric mismatch between the probe signal and the data signal equation (2.6) becomes

$$P_{pc}(\cdot, \Delta) = \sum_{i=1}^I G_{\omega}(R + \Delta r, z_0 + \Delta z_0, z_i + \Delta z_i) G_{\omega}^*(R, z_0, z_i) \quad (2.11)$$

where Δ represents the geometric mismatch, e.g Δr represents the source-array range change while Δz_0 and Δz_i represent the source and the array depth changes, respectively.

In order to compensate for this mismatch, a frequency shift is applied to the data signal and convolved with the mismatching probe signal IR so equation (2.11) becomes

$$P_{pc}(\cdot, \Delta, \Delta\omega) = \sum_{i=1}^I G_{\omega}(R + \Delta r, z_0 + \Delta z_0, z_i + \Delta z_i) G_{\omega + \Delta\omega}^*(R, z_0, z_i). \quad (2.12)$$

If the geometric mismatch is only due to range shift then equation (2.10) becomes

$$\Delta\omega_r = -\frac{\omega}{R} \Delta r \beta, \quad (2.13)$$

where $\Delta\omega_r$ is the frequency shift required for source-array range change compensation. In [8] the range variability concept is extended to source and array depth through

$$\Delta\omega_0 = -\frac{\omega}{R} \Delta z_0 \zeta_0, \quad (2.14)$$

$$\Delta\omega_i = -\frac{\omega}{R} \Delta z_i \zeta_i, \quad (2.15)$$

where ζ_0 and ζ_i are the waveguide invariants for the source depth and array depth, respectively. These waveguide invariants are dependent on the sound speed profile and water column depth. In case of more than one variable effect (source-array range, source depth or array depth), the resulting frequency shift is given by

$$\Delta\omega = \Delta\omega_r + \Delta\omega_0 + \Delta\omega_i. \quad (2.16)$$

2.3 Description of the UAB'07 experiment

The communication experiment conducted during UAB'07 aimed at field testing FSpTR. The FSpTR minimizes the MSE by taking in consideration the properties that are varying during data transmission. In its present implementation, the FSpTR allows for the compensation of the source/receiver depth and source/receiver range variations by acting as an adaptive matched filter as shown in figure 2.1. The experiment described in this work was specifically designed for demonstrating, with real data, that source depth variations results in a channel IR frequency shift and the knowledge of such frequency shift can be used to improve the performance of the communication system.

Figure 2.2 shows the underwater environment during the experiment. This diagram is an approximation of the bottom environment as the exact bathymetry map was not available. During the experiment, the source was suspended by a crane from a fixed platform, 10 m from shore, at an initial depth of 5 m. The receiver was a Vertical Line Array (VLA) with 16 hydrophones uniformly spaced at 4 m between 6 m to 66 m depth. The communication range was approximately 1 km with the bottom depth 12 m at source location to about

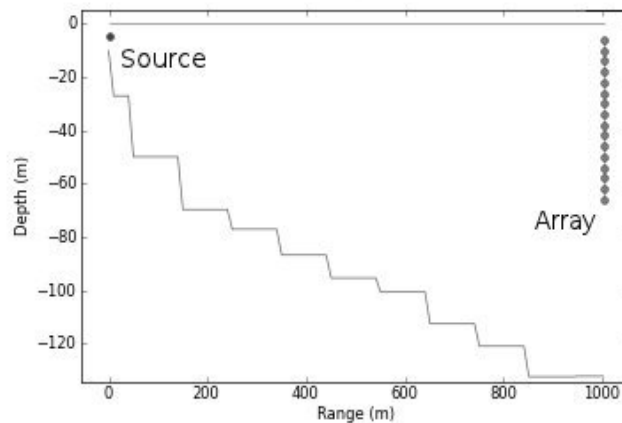


Figure 2.2: modeled source/array transect.

120 m at array location. A carrier frequency of 6250 Hz was used. The transmitted signal comprised of 50 chirp signals followed by a data set of 100 seconds. The chirp transmission was used for the channel IR estimation and to study the channel variability and the Doppler spread. Each chirp has a bandwidth of 2 KHz ranging from 5.5 to 7.5 kHz with 0.1 sec duration whereas data bandwidth ranges from 5.5 to 7.5 kHz with PSK-2 modulation and baud rate of 1000 bits/sec.

Figure 2.3 shows the sound speed profile during the experiment. It is clearly visible from the diagram that the middle part of the water column is constant in terms of velocity than the top and bottom. In order to exploit this stability in the sound speed profile, only the first ten hydrophones are used for the processing of FSpTR, which span upto 42 m of the water column depth. Figure 2.4 (a) shows the IR estimates obtained by the correlation of the chirp signal with the received data. Two strong arrivals can clearly be seen which are followed by the combination of an unstructured multipath. The Doppler spread of the channel is shown in Fig. 2.4 (b) where it can be seen that the Doppler spread of the channel spans upto 20 Hz. The Doppler spectrum is very complex, which illustrates the variability of the underwater channel.

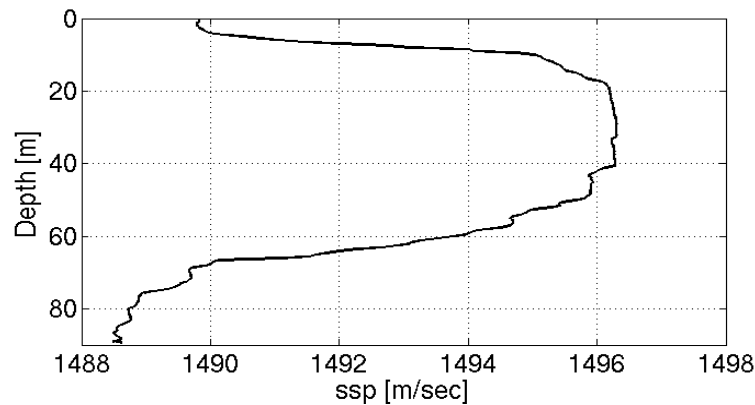


Figure 2.3: sound speed profile, CTD measured by the research vessel Gunnerus.

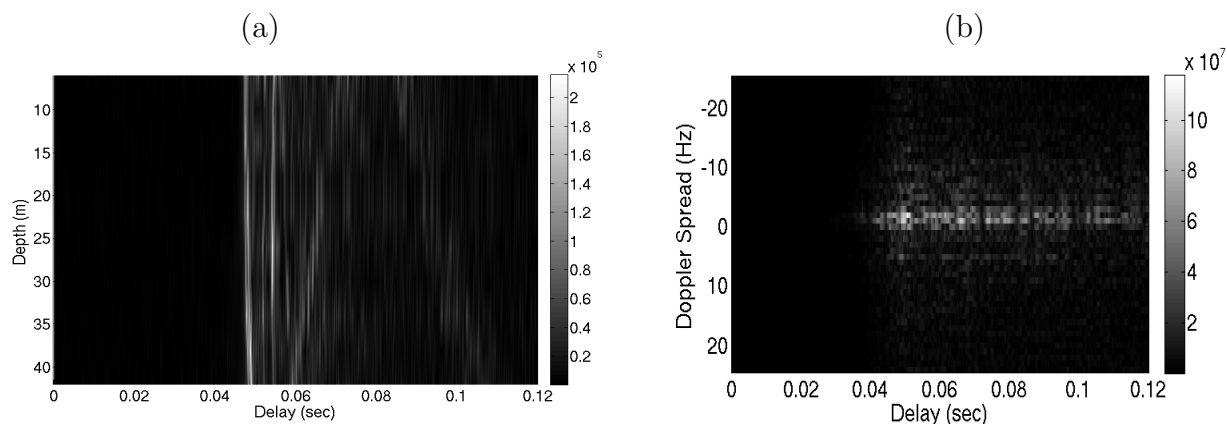


Figure 2.4: underwater channel characterization, a) arriving patterns estimated by pulse compression, b) Doppler spread of the channel during the 15 seconds, calculated at the 5th hydrophone.

During the experiment, the source depth was changed at known instants of time by using a crane. This was called a YOYO experiment and is shown in Fig. 2.5 where the time axis illustrates the time starting from 12:40 pm. In the next section the processed data sets 1 and 2 are presented whose time instants are shown in Fig. 2.5. The data collected from the sea trial is processed in the following steps: i) applying a band pass filter, ii) converting to base band by applying carrier frequency shift iii) obtaining IR estimation by pulse compression iv) saving IR and data in separate folders for further processing. Both the IRs and the data are then fed to the FSpTR equalizer.

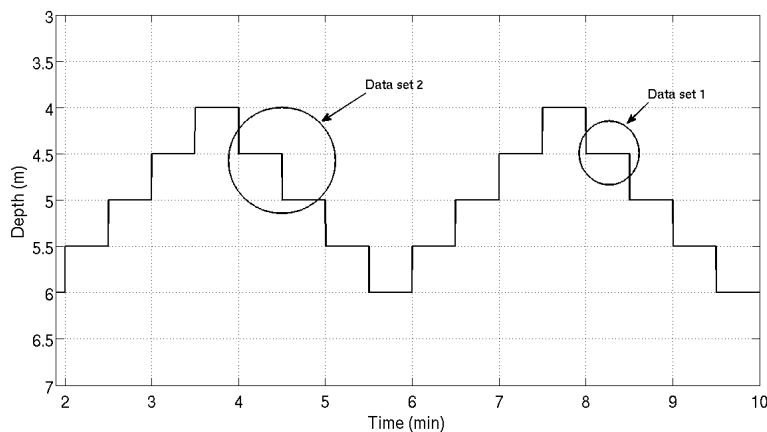


Figure 2.5: YOYO experiment: source depth variations over time. Start time is 12:40 pm.

2.4 Results and observations

The first data set is taken between 12:45 pm to 12:46 pm, as indicated in Fig. 2.5. During this time interval the source depth is changed from 4 m to 4.5 m. Figure 2.6 shows the result of the initial 30 sec of the FSpTR output power associated with the frequency shift ranges from -600 Hz to 200 Hz. It can be seen that the frequency shift which gives the maximum power, changes from approximately 0 Hz to approximately -350 Hz after 6 sec to compensate for the depth shift at that time. In Fig 2.7 the performance comparison between pTR (solid line) and FSpTR (dashed line) is shown in terms of MSE. It can clearly be seen that the frequency shift compensates for the depth shift since the MSE performance of the FSpTR is

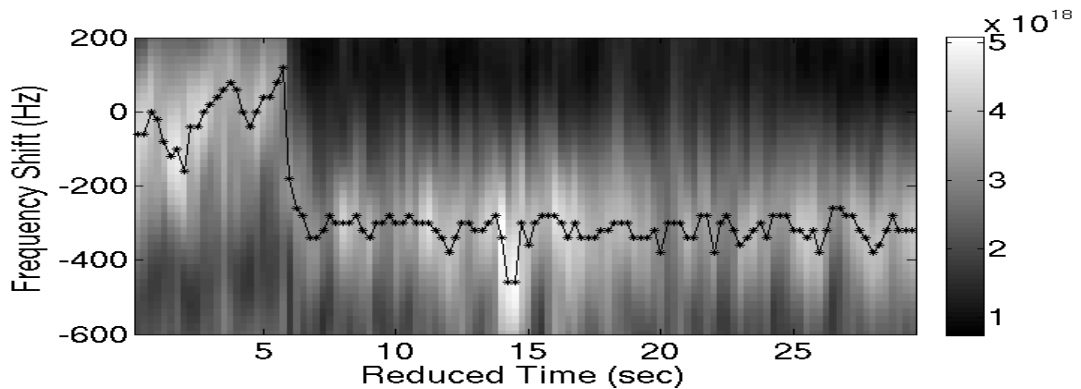


Figure 2.6: FSpTR mean power as a function of time and frequency shift for 10 hydrophones (data set 1).

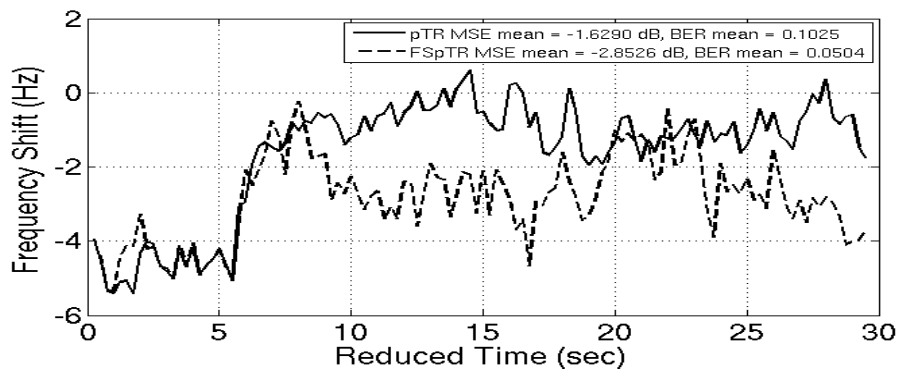


Figure 2.7: MSE comparison between FSpTR and pTR for 10 hydrophones with the source depth shift at 6 sec (data set 1).

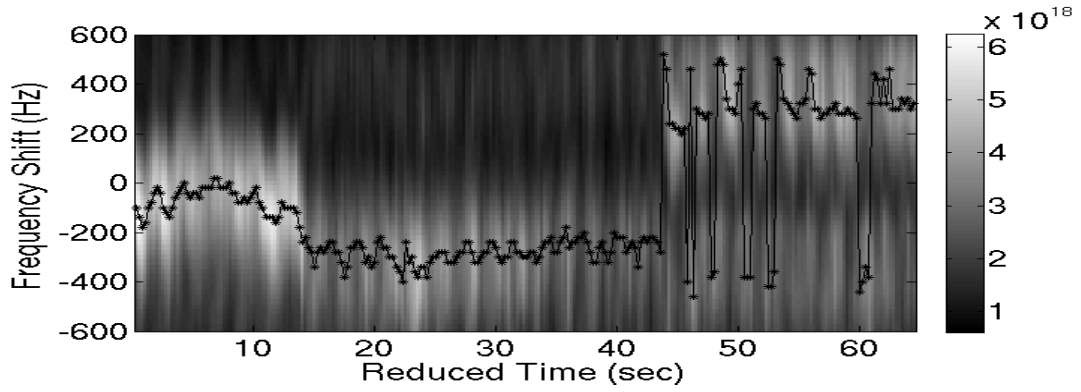


Figure 2.8: FSpTR mean power as a function of time and frequency shift for 10 hydrophones.

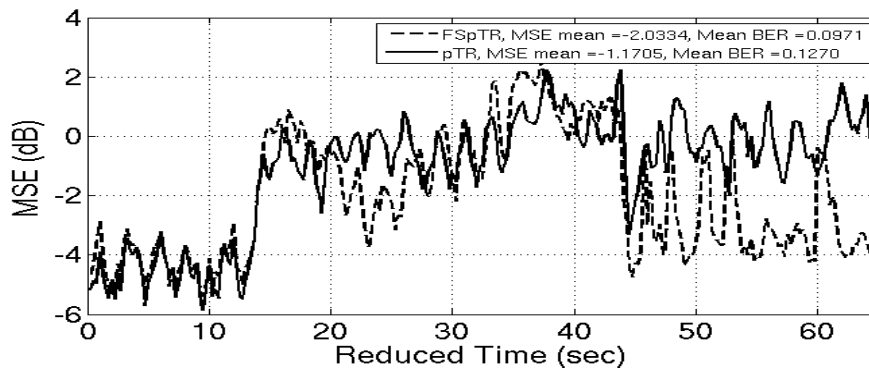


Figure 2.9: MSE comparison between FSpTR and pTR for 10 hydrophones with the source depth shifts at 12 sec and 42 sec.

significantly better than the pTR after 6 sec. During the whole 30 sec there is a mean MSE gain of 1.2 dB that results in an improvement in BER from 10% to 5%.

The same procedure is applied to data set 2 taken between 12:42 pm and 12:43 pm in which there were two depth shifts from 4 to 4.5 m and 4.5 to 5 m at 12 and 42 sec respectively as shown in Fig. 2.5. The results are shown in Fig 2.8 and 2.9. In Fig 2.8, the FSpTR equalizer successfully tracks the two source depth changes and applies the appropriate frequency shifts, which are from 0 Hz to approximately -350 Hz for 4 m to 4.5 m and from -350 Hz to 350 Hz approximately for 4.5 m to 5 m. Figure 2.9 shows the performance comparison in terms of MSE for pTR (solid line) and FSpTR (dashed line). It is interesting to note that in both cases, for a depth shift of 4 m to 4.5 m, FSpTR selects the same frequency shift *i.e.* 350 Hz,

but in the second case the FSpTR equalizer does not compensate for this source depth. On the other hand while analyzing the performance only after the second depth shift, from 4.5 m to 5 m, the FSpTR equalizer compensates very well and there is a mean gain of about 1.8 dB in MSE and BER improvement from 17.1% to 9.2% . During the whole 65 sec there is a mean MSE gain of 0.8 dB that results in an improvement in BER from 12% to 9%. The lack of improvement in performance in the first part of the FSpTR output is an open question, which requires further investigation.

2.5 Conclusion

In this chapter, an environment based pTR equalizer (FSpTR) is presented which compensates for some of the unpredictable changes in the underwater environment such as source and array depth changes. The FSpTR is then tested with real data collected during the UAB'07 experiment. The results have shown that the FSpTR successfully tracked source depth changes.

The environment based equalizer presented in this chapter is based on the waveguide invariant properties of the underwater channel. It is shown in [8] that an effective number of modes corresponds to a specific waveguide invariant. From (2.13), which relates the waveguide invariant to the frequency shift, it can be seen that for a proper compensation of environmental variations different frequency shifts should be applied for different group of modes [8]. In a ray analogy, for a perfect waveguide, each mode is associated to a specific path from the transmitter to the receiver which is characterized by its angle of arrival[13]. In order to improve the performance of the communication system different frequency shifts should be applied corresponding to different paths *i.e.* different group of modes. This problem will be

addressed in detail in chapter 4.

Chapter 3

Doppler decomposition of underwater acoustic channel

3.1 Introduction

Most underwater acoustic systems and applications are greatly affected by source/receiver motion and surface variations. Due to these variations the underwater channel changes strongly with time. In order to improve the performance of underwater acoustic communications, it is important to design new techniques to track these changes. The main idea of this chapter is to address this problem and propose a new method to infer information about these perturbations based on Doppler analysis. In addition it is also shown that due to the environmental perturbations each path is affected by a different Doppler. In chapter 2 an environment based equalizer, called Frequency Shift Passive Time Reversal (FSpTR), was discussed in detail which compensates for the environmental variations by applying an appropriate frequency shift. From the Doppler analysis presented in this chapter it will be deduced that a single frequency shift will not be sufficient to compensate for all environmental variations, thus different frequency shifts would be required to compensate for these variations.

The underwater acoustic channel is characterized by a long multipath spread where each

path is subject to distortion due to the motion of the transmitter and/or the receiver, the sea surface and other environmental variations. In recent literature many studies focus on the simulation of the sea surface variations and their effects on the Doppler spread spectrum. In [40] two simulation methods are described for modeling time varying sea surface using ray theory and ray based formulation of the Helmholtz integral equation with a time domain Kirchoff approximation. In [41] a matched filtering technique is used to estimate the Impulse Response (IR) and to study the effect of environmental variations caused by source/array movement and sea surface motion on the IR. In both [40] and [41] the Doppler shifted replicas of the transmitted signals are matched filtered with the received signal and depending on the peak in the ambiguity plane source/receiver motion and surface variations are estimated.

Due to source and/or receiver motion and surface variations each path is affected by different dynamics of the environment. To study the effect on each path, a Time Windowed Doppler Spectrum (TWDS) is used. TWDS is computed by windowing the IR over time. Computing TWDS along time revealed that the Doppler spectrum varies due to environmental perturbations. In this chapter the TWDS technique is applied to real data acquired on a single hydrophone and variations in Doppler are clearly found. A time-frequency based technique similar to the one proposed in [49], is used to improve the resolution of the results and to see the temporal evolution of Doppler on the direct arrival and on the surface reflected arrival over the transmission time.

The real data of CALCOMM'10 sea trial is presented in this chapter. CALCOMM'10 took place on the south coast of Portugal from 22nd to 24th of June 2010. The data set presented in this chapter has a duration of 15 sec and contains chirp signals with the central frequency

of 3.125 kHz, duration of 0.1 sec and a repetition rate of 0.3 sec. A similar scenario is also modeled using the Bellhop model [50]. By computing the ray tracing diagram it is observed that the first arrival is the combination of the direct path and surface reflected path, reaching the hydrophone at the same time which results in a destructive interference at the receiver. Due to their simultaneous arriving time it is not possible to distinguish the arrivals in the estimated IRs, however since the arrivals are affected by different environmental dynamics it will be shown that they can be separated in the Doppler domain.

The chapter is organized as follows: section 3.1 elaborates the theoretical background and mathematical modeling of the problem. Section 3.2 gives the description about the CAL-COMM'10 sea trial. Section 3.3 explains modeling results with bellhop ray tracing model simulation and some preliminary results. Section 3.4 presents the data processing and results with the real data and Section 3.5 presents the conclusions.

3.2 Theoretical Background

In underwater transmission/reception systems, the transmitted signal reaches the hydrophone through different paths which can be categorized as the surface reflected, bottom reflected and water column refracted paths. The water column refracted paths are mostly direct paths which are affected by the sound speed profile which is a function of depth and range. Each of these paths has different sensitivities to the environmental variations. The water column refracted paths are only sensitive to the source and array motion while the surface reflected path is also affected by the surface motion in addition to the source and array motion.

The geometric variations like source/array movements produces compression/expansion in the transmitted signal which induces different Doppler in each arriving path. This can be

analyzed at the path level in terms of time-variable IR h_{ip} for a single propagation path p , in [43] it is shown that

$$h_{ip}(t, \mu) = g_{ip}\left(\mu + (t - \mu)\frac{v}{c}\right)e^{j\omega_c\left(\mu + (t - \mu)\frac{v}{c}\right)}, \quad (3.1)$$

where $g_{ip}(t, \mu)$ is a single path, p , propagating between the source and the hydrophone i , transmitted at an instant t and received at the hydrophone after a delay μ . Due to the channel properties variability the length, $l_p(t)$ of the path changes with a velocity $v = \partial l_p(t)/\partial t$. The ratio between such velocity and the sound speed, c , induces a delay variation in the $g_{ip}(t, \mu)$ argument and a frequency shift given in (3.1) by the complex exponential. Such frequency shift is responsible for the Doppler spread that also depends on the central frequency, ω_c , of the narrowband transmitted signal. Equation (3.1) gives the time variable IR for a single path which can be generalized to p paths by doing a weighted sum of all the delayed replicas of the transmitted signal,

$$h_i(t, \mu) = \sum_p h_{ip}\delta(\mu - \mu_{ip}), \quad (3.2)$$

where $h_i(t, \mu)$ incorporates all the Doppler experienced by the i^{th} hydrophone of the array due to all arriving paths. To compute the Doppler corresponding to each hydrophone, a Fourier transform is taken with respect to time in equation (3.2) which gives the spreading function $H_i(\phi, \mu)$ as

$$H_i(\phi, \mu) = \int_{-\infty}^{\infty} h_i(t, \mu)e^{j2\pi\phi t} dt, \quad (3.3)$$

where ϕ is the Doppler axis.

Figure 3.1 shows the simplified ray diagram showing two paths p_1 and p_2 from the source T

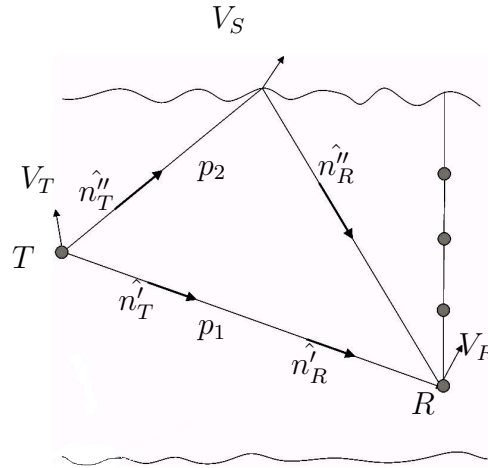


Figure 3.1: Two arriving paths from transmitter to the receiver, path p_1 is the direct path and path p_2 is the surface reflected path. V_T , V_R and V_S are the constant velocity vectors at the transmitting, receiving and the surface reflection point respectively. The unit vectors \hat{n}'_T and \hat{n}'_R represents the directions of the propagation of the transmitted and received signal for the direct path while \hat{n}''_T and \hat{n}''_R represents the unit vectors for the surface reflected path.

to the hydrophone R . Path p_1 is the direct path from the source to the receiver while path p_2 is the surface reflected path. Considering only the surface induced motion, path p_1 is only affected by the up-down and range movement of the surface suspended array while p_2 is directly affected by the surface motion as well as the array motion. In figure 3.1, V_T , V_R and V_S are the constant velocity vectors at the transmitting, receiving and the surface reflection point respectively. \hat{n}'_T and \hat{n}'_R are the unit vectors in the directions of the propagation of the transmitted and received signal for the direct path while \hat{n}''_T and \hat{n}''_R are the unit vectors for the surface reflected path.

The change in path length is a function of velocity so the Doppler is induced in both paths by the source motion and the surface motion which is given by [51]

$$\phi_A = -(1 - s)f_c, \quad (3.4)$$

where ϕ_p is the actual Doppler shift in hertz for a single path, f_c is the carrier frequency and s is the time compression/expansion factor given by

$$s = \frac{(1 - V_S \cdot \hat{n}_T/c)(1 - V_R \cdot \hat{n}_R/c)}{(1 - V_S \cdot \hat{n}_R/c)(1 - V_T \cdot \hat{n}_T/c)}. \quad (3.5)$$

For path p_1 the compression/expansion factor s' is given by

$$s' = \frac{(1 - V_R \cdot \hat{n}'_R/c)}{(1 - V_T \cdot \hat{n}'_T/c)}. \quad (3.6)$$

Substituting this value in equation (3.4), the actual Doppler ϕ'_1 becomes

$$\phi'_1 = \frac{(V_T \cdot \hat{n}'_T - V_R \cdot \hat{n}'_R)/c}{1 - V_T \cdot \hat{n}'_T/c} f_c. \quad (3.7)$$

Equation (3.7) relates the actual Doppler shift ϕ_1 with the relative velocities of the source and the hydrophone. Considering a static hydrophone, when the source is moving away from the hydrophone then $\hat{n}'_T = -\hat{n}'_R$ and $\phi'_1 < 0$. When the source moves towards the hydrophone one can get that $\hat{n}'_T = \hat{n}'_R$, and $\phi'_1 > 0$.

Solving (3.4) for path p_2 one can get that

$$\phi'_2 = \frac{((V_T - V_S) \cdot \hat{n}''_T - (V_S - V_R) \cdot \hat{n}''_R)/c}{(1 - V_S \cdot \hat{n}''_R/c)(1 - V_T \cdot \hat{n}''_T/c)} f_c. \quad (3.8)$$

where $(V_T - V_S)$ and $(V_S - V_R)$ are the resulting velocities due to the source and the hydrophone velocity and the surface velocity V_S . So, (3.8) shows the effect of the surface variations on Doppler shift ϕ'_2 for the surface reflected path. Similar analysis can be made

in terms of the Doppler shift and the relative motion of the source and the hydrophone. Considering a static hydrophone, when path p_2 gets larger $\hat{n}_T'' = -\hat{n}_R''$ * and $\phi_2' < 0$. When path p_2 gets shorter $\hat{n}_T'' = \hat{n}_R''$, and $\phi_2' > 0$.

3.3 Experimental description

The data analyzed in this chapter was collected during the CALCOMM'10 experiment, which took place off the south coast of Portugal, about 12 nautical miles south east of Vilamoura, from 22nd to 24th of June 2010. The main objectives of the experiment were to collect field calibration data for tomography purposes, to transmit communication signals in different frequency bands, to analyze the performance of underwater communication systems and to study its environmental variation dependence.

The acquisition system used for gathering the data comprised two free drifting acoustic oceanographic buoys (AOBs), one with 8 hydrophones and the other with 16 hydrophones [52].

The data presented in this chapter was taken on Day 2 of the experiment from the 16 hydrophone array in which all the hydrophones are equally spaced at 4 m. The results presented in this chapter were acquired from the communication signals which comprises LFM's and QPSK modulated signals. Some details about the different transmitted signals during the experiment are shown in table 1.

Figure 3.2 (a) shows a downward refracting sound speed profile measured during the experiment. Figure 3.2 (b) shows the source and receiver locations during data transmissions plotted over the bathymetric map of the area where the experiment took place. During

*This can be understood with the help of the image method, proposed in [12]

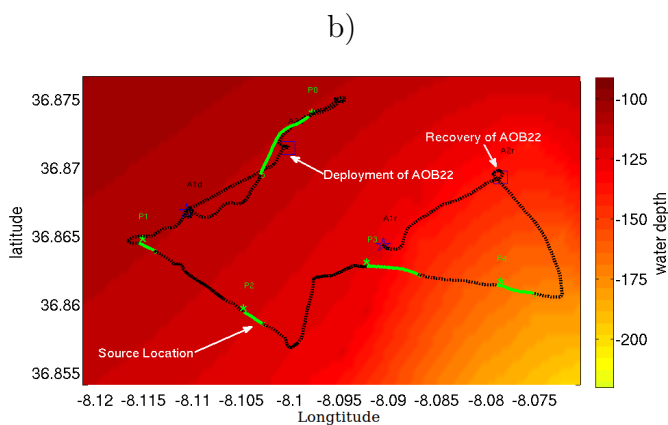
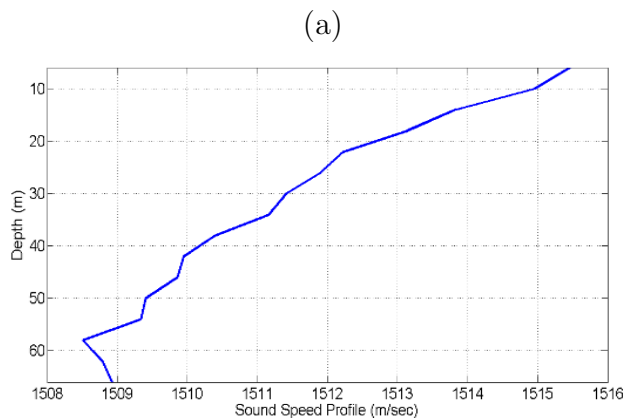


Figure 3.2: (a) downward refracting sound speed profile during Day 2 (b) Day 2 bathymetry map of the work area with GPS estimated locations of AOB21 and AOB22 deployments and their recovery, ship/source track (dotted lines) and ship track during communication events (green lines).

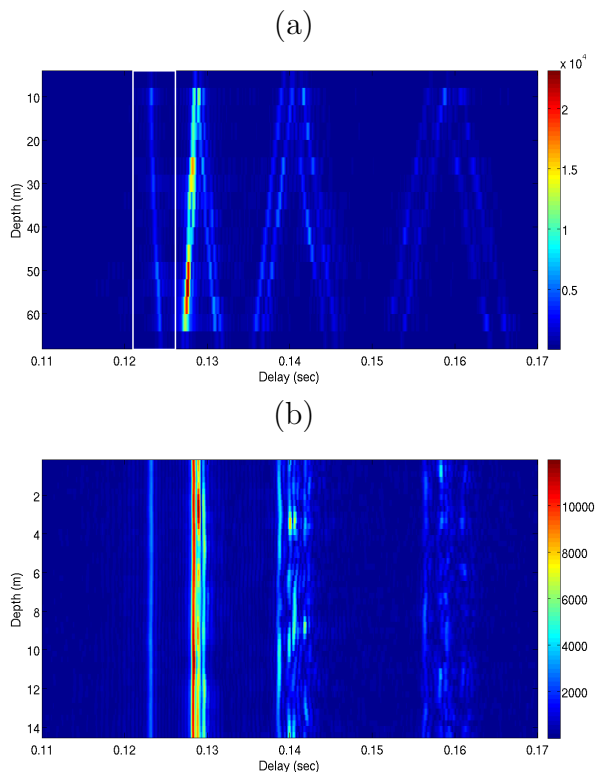


Figure 3.3: IR estimates: (a) for 16 hydrophone array and white lines showing the selected wavefront (b) the temporal evolution of IR along 15 sec of transmission for channel 3.

the data transmission analyzed in this chapter, the source array distance was around 850 m with a downslope bathymetry, the source was located at about 12 m depth and the first hydrophone of the array was located 6.3 m from the surface.

3.4 Preliminary observations

The discussion of this section is mainly focused on the low frequency chirps (LF_AERU1 code, see table 1) with the central frequency of 3.125 kHz. The received chirps were first filtered by a band pass filter to remove out of band noise, then the filtered signal was converted to baseband and pulse compressed with the transmitted chirps to get the channel IR estimate. Figure 3.3 (a) shows the estimated arriving pattern that comprises an impulse reaching the array of hydrophones through different paths and (b) shows the temporal evolution of the IR at hydrophone 3 along the 15 sec of chirp transmission.

In figure 3.3 (a) two abnormalities can be observed. It is expected to see a strong (high energy) arrival which can be due to direct path between the source and the array but this is not the case in this scenario. The first wavefront has lesser energy as compared to the

Table 3.1: Signal Specification for the CALCOMM'10 Experiment

Code	Type	Baud Rate (bps)	Start-stop freq (KHz)	Duration (sec)
LF_AERU1	LFM	-	2.64-3.75	0.1
MF_AERU1	LFM	-	5.0-7.0	0.1
MF_PASU1	LFM	-	5.0-7.0	0.1
HF_PASU1	LFM	-	10.0-15.0	0.1
LF_AERU2	QPSK	500	2.9-3.5	30.2
MF_AERU2	QPSK	1000	5.5-7.0	30.2
MF_PASU2	QPSK	1000	5.5-7.0	30.2
HF_PASU2	QPSK	2000	11.0-14.0	30.2

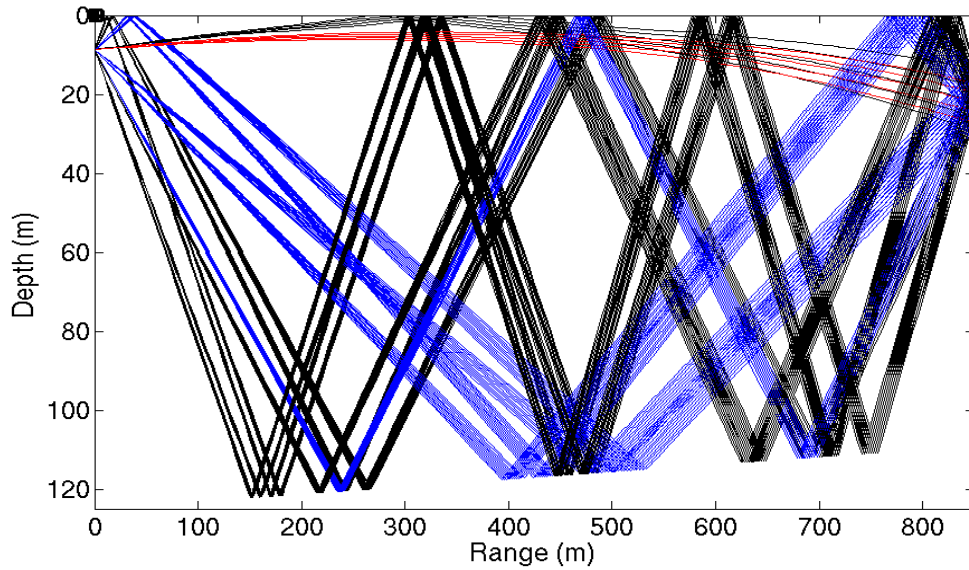


Figure 3.4: ray tracing diagram of the signal propagation over the environment of CALCOMM'10

second wavefront. Secondly the second high energy wavefront has a positive slope so the signal is reaching the bottom hydrophone first which suggests that this is a bottom reflected wavefront. The source is located very near the surface so the surface reflected wavefront should reach the hydrophones before the bottom reflected wavefront. The reason for these abnormalities can be explained by modeling the environment with the Bellhop propagation model.

Figure 3.4 shows a Bellhop simulated ray tracing diagram for the environment. By analyzing the path delay it can be seen that the direct arrivals (red lines) and the surface reflected arrivals (black lines) are reaching the hydrophone at the same time so the first wavefront is the superposition of the direct and the surface reflected arrivals. Due to the reflection from the surface the phase of the surface reflected arrival changes which results in a destructive interference of the surface reflected arrival and the direct arrival resulting in a strong power reduction.

3.5 Data processing and results

In section 3.2 it was shown that each arrival is affected by different dynamics of the environment that induces a different Doppler shift for each arrival. The direct arrival is affected by the source and the hydrophone motion while the surface reflected arrival is affected by source motion, hydrophone motion and the surface motion. With the objective of analyzing the environmental dynamics on each arrival, a method based on Doppler analysis is presented. Figure 3.5 (a) shows the zoomed version of the first path in figure 3.3 (a) which corresponds to a delay of 0.124 sec. In this figure it is not possible to extract any information regarding the number of the arrivals. Figure 3.5 (b) shows the corresponding Doppler spread of the

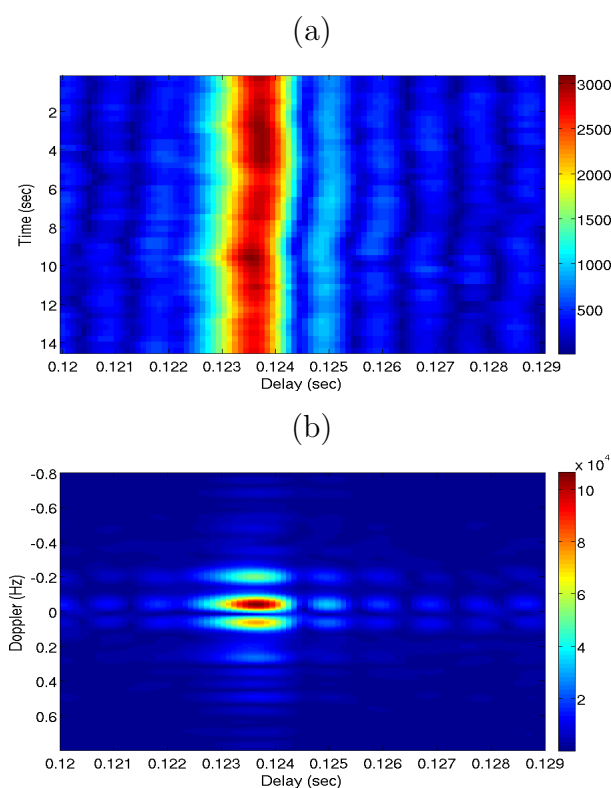


Figure 3.5: (a) variability of the selected wavefront shown in figure 3.3 (a), (b) corresponding Doppler spread of the selected wavefront

first wavefront. Three lobes are clearly visible in the figure. The middle lobe at ~ -0.01 Hz is assumed to be due to the main arrival. Some ambiguity persists regarding the other two side lobes at 0.1 Hz and -0.2 Hz as they may be due to two different arrivals or a single arrival which is affected by different dynamics of the environment. However if the two side lobes are due to a single arrival then the two lobes should not appear simultaneously in a short time slot Doppler analysis.

In order to clarify the origin of the two side lobes Time Windowed Doppler Spectrum (TWDS) is used to study the temporal evolution of the selected wavefront. TWDS is computed by windowing the IR estimate, shown in figure 3.5 (a), along time and computing the Doppler for the corresponding window of the IR. A root raised cosine window is used for windowing in this analysis because of its capability in reducing the side lobes due to the windowing effect. TWDS for an input signal $x(t)$ can be shown as the short time Fourier transform of a signal [53]

$$S(t, \omega) = \int_{-\infty}^{\infty} x(t)w(t - \tau)e^{-j\omega\tau} d\tau \quad (3.9)$$

where $w(t)$ is the window function which is root raised cosine function in this case.

Figure 3.6, 3.7 and 3.8 (a) show the TWDS results computed with a window of 4 sec and a roll-off factor of 0.5, where the window slides 0.5 sec from figure 3.6 to 3.7 and to 3.8. Figure 3.6, 3.7, 3.8 (b) show the corresponding Doppler spread summation along the delay axis. The following observations can be made from these figures; (i) figure 3.6 (a) shows a main spot at -0.01 Hz and a relevant side spot at ~ 0.5 Hz; (ii) figure 3.7 (a) shows a main spot at 0.1 Hz and two side lobes at approximately -0.4 Hz and 0.5 Hz, and (iii) figure 3.8 (a) shows the main spot at 0.1 Hz and the side spot at 0.4 Hz. In all cases the main spot is

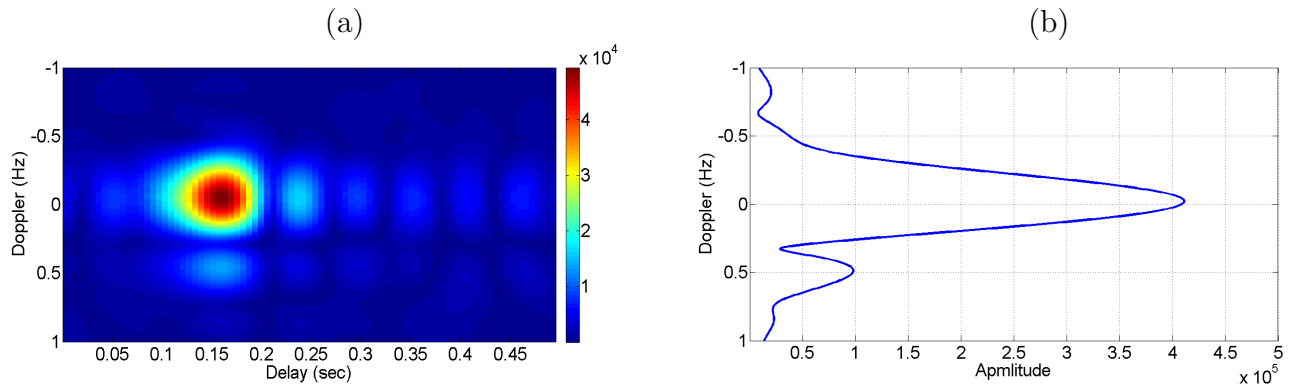


Figure 3.6: (a) Doppler computed only for 4 sec time window, centered at 4.5 sec, where two lobes can be seen; the first due to one main arrival at ~ 0.01 Hz and the second due to the surface reflected arrival at approximately 0.5 Hz (b) Doppler summation along the delay axis

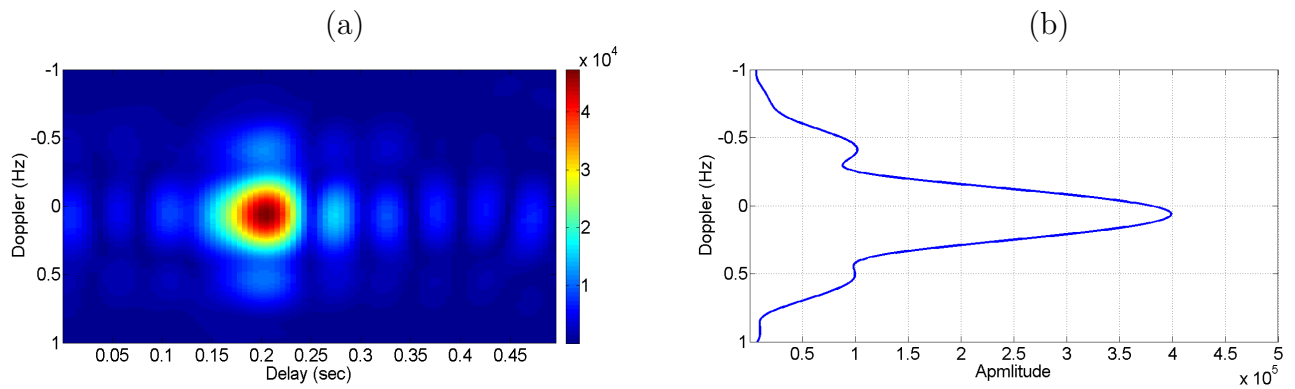


Figure 3.7: (a) Doppler computed only for 4 sec time window, centered at 5.5 sec, where three lobes can be seen; the first due to the main arrival at ~ 0.1 Hz and the other two due to the surface reflected arrival at ~ -0.4 Hz and ~ 0.5 Hz (b) Doppler summation along the delay axis

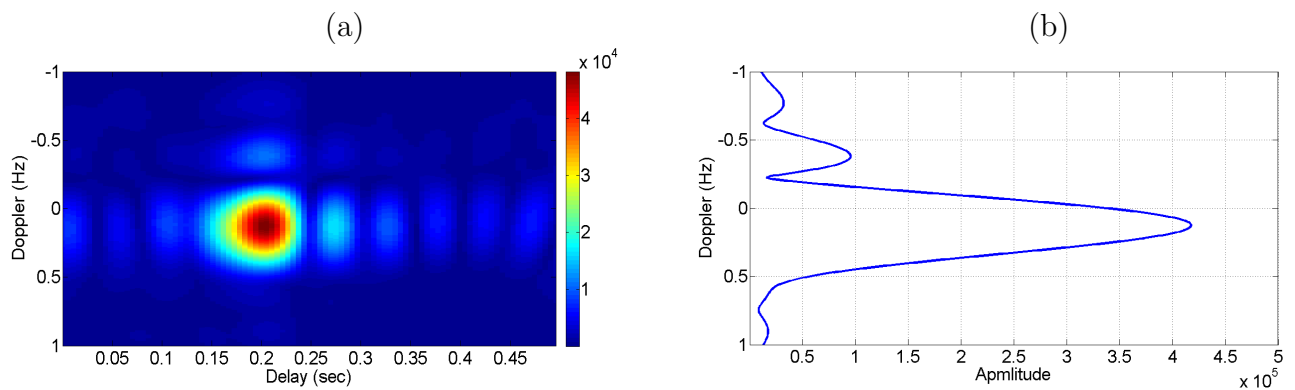


Figure 3.8: (a) Doppler computed only for 4 sec time window, centered at 6.5 sec, where two lobes can be seen; the first due to the main arrival at ~ 0.1 Hz and the second due to the surface reflected arrival at ~ -0.4 Hz (b) Doppler summation along the delay axis

expected to be due to the direct path (p_1 in figure 3.1) which gives different Doppler values due to the array motion for the 3 different windows, nevertheless with the values around zero. The side spots are expected to be due to the surface motion that makes the surface reflected path (p_2 in figure 3.1) larger and shorter, in the following manner : in case (i), the Doppler value is positive revealing that for that window the surface wave is moving up and the path is becoming larger; in case (iii) the Doppler value is negative revealing that for that window the wave is moving down and the path is becoming shorter; and for case (ii) there are two side lobes one negative and the other positive revealing that for that time window the surface wave is crossing a crest, where the path is becoming larger before the crest and becoming shorter after the crest.

Figure 3.6, 3.7 and 3.8 (b) shows the summation of the figure 3.6, 3.7 and 3.8 (a) respectively, along the delay axis to show the Doppler effect more clearly. Figure 3.9 (a) shows the accumulation of figure 3.6, 3.7 and 3.8 (b), showing the summation along the delay axis of the Doppler-delay diagram, for the whole 15 sec of transmission for hydrophone 3. The main idea is to show the complete evolution of Doppler along time. An interesting thing to observe is the variation in the Doppler due to the direct arrival. The direct arrival is only affected by the source and hydrophone motion so it is expected that this variation is due to the source motion but the source is suspended from the surface so the direct arrival is also affected by the surface motion which can be seen in figure 3.9. Secondly due to the windowing effect, the image (mainly for the side lobes) becomes very blur, so it is difficult to identify the Doppler due to the surface motion. This blurring effect is due to the resolution trade-off which is one of the drawbacks of TWDS.

Resolution trade-off suggests that in order to get a good time resolution a narrow window in

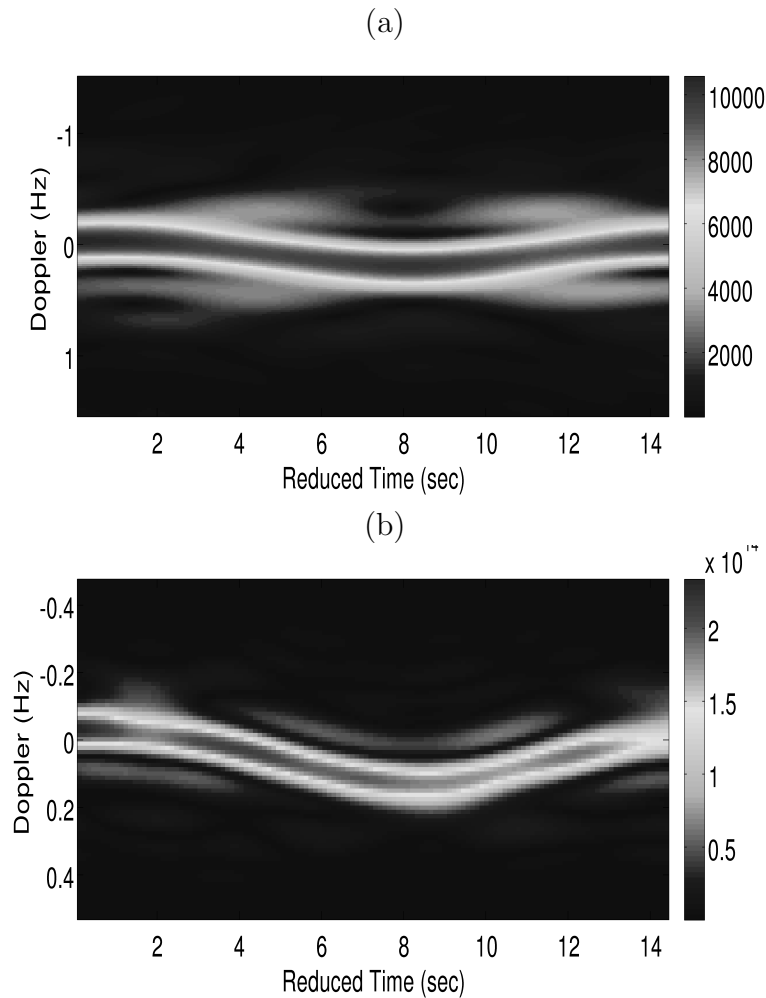


Figure 3.9: (a) summation along the delay axis of Doppler-delay diagram computed by only TWDS analysis (b) summation along the delay axis of Doppler-delay diagram computed by combination of TWDS and WT.

time domain $w(t)$, is required while for good Doppler domain resolution a narrow frequency domain window $W(\omega)$ is required in Doppler domain. But both $W(\omega)$ and $w(t)$ can not be optimized at the same time to get a good resolution in both time and Doppler domain. In order to improve the resolution, Time Frequency (TF) analysis technique, proposed in [49] is used.

This technique helps in overcoming the resolution trade-off by using a Wigner Transform

(WT). In [49] the Wigner Transform for input signal $s(t)$ is given by

$$S(t, \omega) = \int_{-\infty}^{\infty} s^* \left(\frac{t - \tau}{2} \right) \cdot s \left(\frac{t + \tau}{2} \right) e^{-j\omega\tau} d\tau \quad (3.10)$$

The Wigner transform gives crisp resolution due to the correlation operation. As proposed in [49], the resolution trade-off can be overcome by simply multiplying TWDS with WT. Figure 3.9 (b) shows the results of this technique for hydrophone 3. By comparing the results in figure 3.9 (a) and (b) it can be observed that the Doppler due to direct arrival and the surface reflected arrival can easily be distinguished. The Doppler values starts from a negative value and two transitions occur at ~ 4 sec and ~ 10 sec.

In this work the environmental variations are observed on the surface reflected arrival. From figure 3.9 (b) it can be seen that different Doppler is induced in the surface reflected arrival at different times. This observation emphasizes the need for a robust arrival based equalizer which compensate each arrival separately in accordance with the environmental variations.

3.6 Conclusion

In this chapter Doppler domain analysis of the underwater acoustic channel is done to analyze the time variability of the channel. In the underwater multipath environment each path is affected by different environmental variations. The effects of these variations can be studied by observing the Doppler variations in the Impulse Response. These Doppler variations are observed due to contraction and expansion in the path length between the source and the receiver. Time Windowed Doppler Spectrum is used to study these effects on the channel impulse response. By isolating a single wavefront and observing its temporal evolution it is revealed that it is composed of two arrivals (direct and surface reflected) interfering

destructively at the receiver. To study the effect of surface motion, the temporal evolution of the Doppler induced in the surface reflected path is studied in detail.

The Doppler analysis presented in this chapter showed that each arrival is affected by the environmental variations in a different manner, resulting in different amount of Doppler in each arrival. In chapter 2, frequency shift passive time reversal (FSpTR) was discussed in detail, which tries to compensate for the channel variations by applying an appropriate frequency. The TWDS analysis revealed that a single frequency shift is not enough to compensate for all the channel variations. In order to improve the performance of the FSpTR system, each arrival must be compensated separately for the environmental variations.

Chapter 4

Beamformed FSpTR for underwater communications

4.1 Introduction

Underwater acoustic communications is an open field of research which offers great challenges due to adverse environmental effects. Achieving reliable underwater communications is still a great challenge due to the strong time varying multipath environment and Doppler spread. Due to these effects the received signal spreads both in the time and frequency domains making equalization a challenging task. The main idea of this section is to use adaptive FSpTR technique along with beamforming processing to improve the performance of pTR-based underwater communication systems.

In chapter 2 it was shown that the FSpTR equalizer can be used to compensate for geometric variations, however the main problem with FSpTR was the selection of optimum frequency shift to compensate for the environmental variations together with the selection of the optimum IR time window. The size of the IR window dictates the number of wavefronts considered by the FSpTR equalizer and each wavefront is affected by the environmental variations in a different manner [8, 48]. The FSpTR equalizer uses a single frequency shift to compensate for these environmental variations thus it fails to compensate for all the envi-

ronmental effects on all wavefronts, resulting in performance degradation of the underwater communication system.

In chapter 3 a technique called Time Windowed Doppler Spectrum (TWDS) was presented which analyze the effects of different environmental variations on each wavefront separately. Real data results have shown that each wavefront is affected by the environmental variations in different manners, which induces different Doppler in each wavefront. These results motivated the idea of using FSpTR for each wavefront separately to compensate for the environmental effects.

In this work beamforming is used to separate different wavefronts that arrive to a vertical line array (VLA) and to allow the compensation of each wavefront variability using the FSpTR technique. Beamforming techniques are used in different underwater applications such as detection and localization of far-field sound sources [54, 55]. The main purpose of using beamforming techniques is to find the direction of arrival of acoustic wavefronts and to enhance the signal to noise ratio of the received signal. The beamforming technique was applied for underwater communications in [56] where a coherent path beamformer (CPB) is proposed for processing the signals using an adaptive processor that forms a beam in the direction of a collection of coherent signals representing the strongest path. In the direction of interference the processor forms a null beam therefore canceling interference within the principal beam [57, 58]. In [59] CPB is combined with a recursive least-square (RLS) filter to further improve the performance of the system. In CPB only the strongest path is enhanced and nulls are placed in all the other paths thus ignoring the energy from the other paths which is a disadvantage, while in this work all the paths are separated by the beamformer, compensated for their time-variation and combined coherently.

In this work the beamformer is integrated with FSpTR so that each wavefront is compensated separately by applying different frequency shifts. This idea is motivated by the fact that in the real multipath environment, each environmental variation affects different arrivals in a different manner so different frequency shifts are required to compensate for the same environmental variation.

The chapter is organized as follows: Section 4.1 will explain the implementation of conventional beamformer with a vertical line array. Section 4.2 will elaborate the proposed approach of combining FSpTR with the beamformer. Section 4.3 will present the complete system diagram and also address some implementation issues. Section 4.4 will present underwater communication results from simulated data and also some real data results and section 4.5 will give the conclusion of the chapter and some future work.

4.2 The beamformer with a vertical line array

The basic purpose of employing beamforming is to spatially filter the space-time field such that the signal from a particular angle is enhanced by constructive combination and signals from other set of angles are rejected by destructive interference. Figure 4.1 elaborates this concept. Figure 4.1 is an extension of figure 1.1 showing the direct, top and bottom paths from the transmitter to the receiver. It also shows the plane wavefronts associated with these paths arriving to the VLA where it can be seen that all wavefronts have different arriving angles thus they arrive at different hydrophones with different delays. It is assumed in this work that the source and the receiver satisfies the far field condition such that the signals are received in the form of plane wavefronts at the receiver. The main idea of using

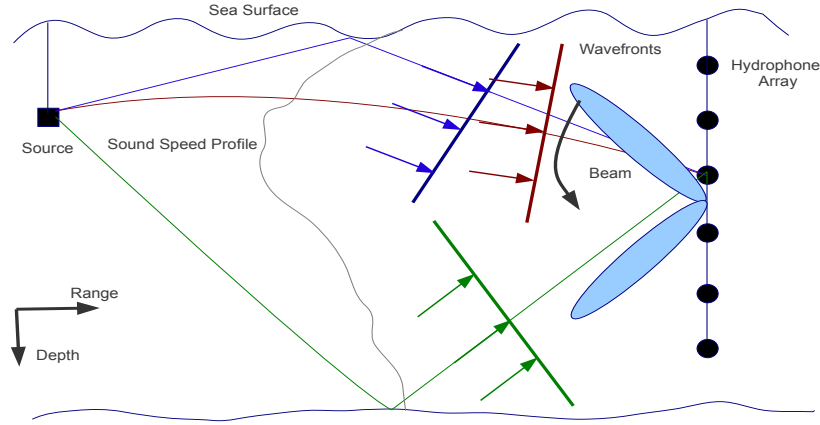


Figure 4.1: basic underwater scenario showing the source, the receiver and different arrivals from the source to the receiver. The VLA beamformer is implemented on the receiver to isolate different arrivals depending on the angle of arrival, by steering the beams along the water column.

a beamformer is to separate these wavefronts arriving at the VLA depending on the angle of arrival.

Figure 4.2 simplifies figure 4.1 showing only a single wavefront reaching the VLA. From the figure it can be seen that the plane wavefront arrives at the each hydrophone of the array with different delays. Let z_i be the depth of each hydrophone in the VLA where i is the hydrophone index and $i = 1, 2, 3, \dots, I$, then the set of received signals at each hydrophone of the array is represented by

$$g(t, z) = \begin{bmatrix} g(t - \tau_1) \\ g(t - \tau_2) \\ \vdots \\ g(t - \tau_I) \end{bmatrix} \quad (4.1)$$

where τ_i represents the delay with which the signal is received at each hydrophone i of the array. It should be noted that the delay encountered by each hydrophone of the VLA is a function of the depth z_i and the angle of arrival θ_k at each hydrophone. The objective of the beamformer is to apply opposite delays τ_i to each hydrophone i of the VLA in order to

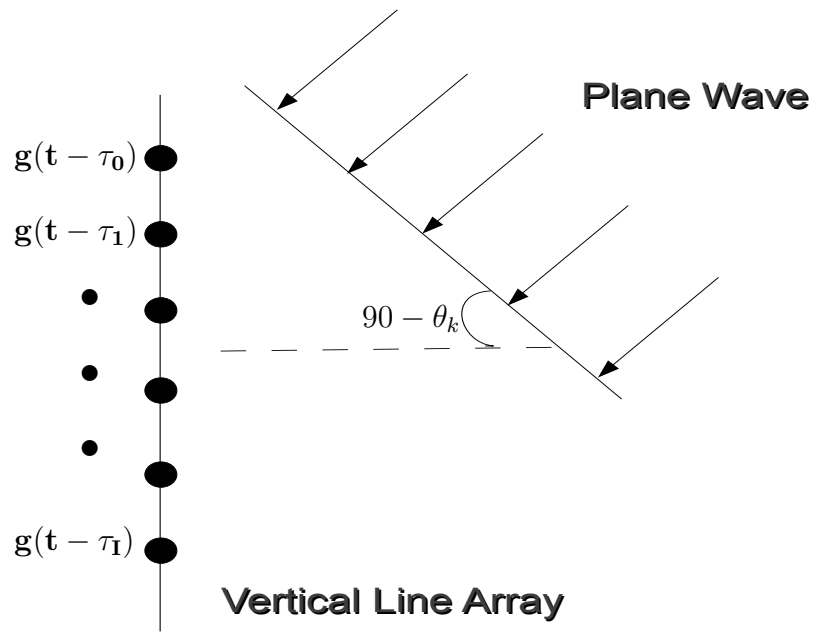


Figure 4.2: Plane Wavefront arriving at each element of the array with different delays

guarantee a coherent summation of the wavefronts in a particular direction.

This is shown in a block diagram in figure 4.3 (a). In the block diagram θ_k is the same for all the hydrophones as it corresponds to the angle of the beam which will be the same

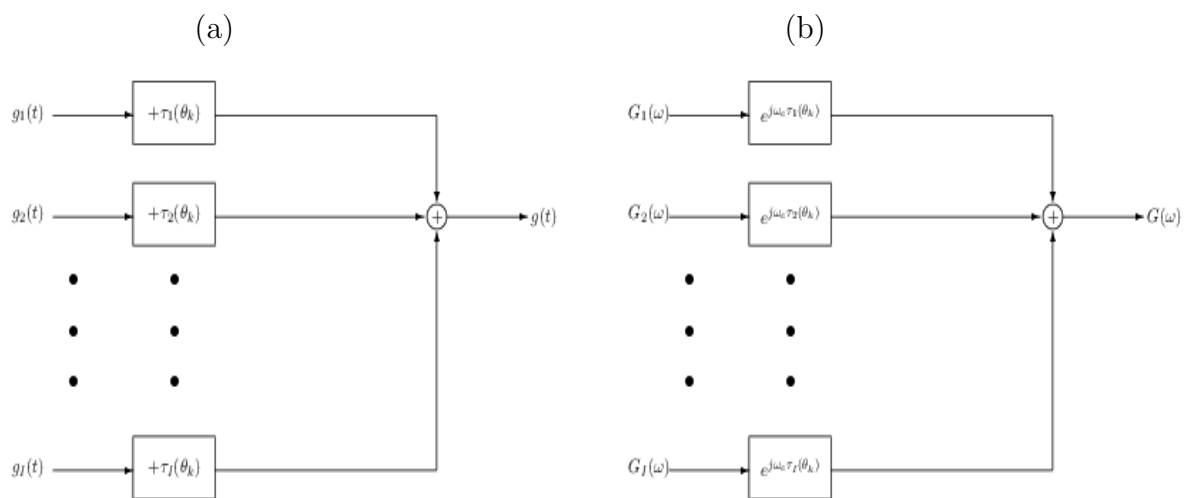


Figure 4.3: Time and Frequency Domain Implementations of the beamformer

for all the hydrophones. However θ_k generates different delays in each hydrophone due to their different depths resulting $\tau(z_i, \theta_k) \equiv \tau_i(\theta_k)$. In the frequency domain the beamformer can be implemented by applying a phase shift to the signal which is done by multiplying an exponential as shown in figure 4.3 (b). This multiplication of exponential is equivalent to applying a delay in the time domain. In this work the frequency domain implementation of the beamformer is used.

As an example, figure 4.4 (a) shows an arriving pattern of a simulated scenario. The

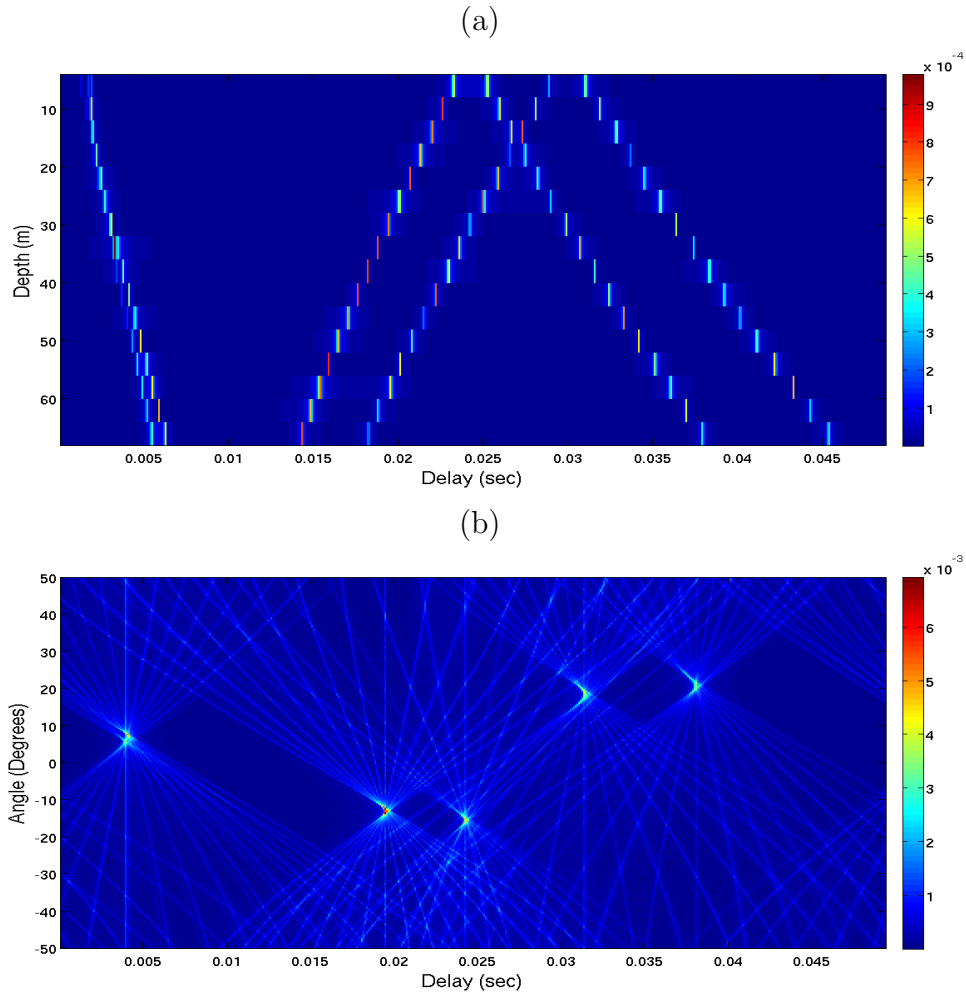


Figure 4.4: simulated channel characterization: a) channel IR estimates b) the beamforming result showing the angle of arrival of different arrivals taking hydrophone 8 as the reference hydrophone, so the delay axis is representing the delay for each wavefront w.r.t hydrophone 8.

source-receiver range is 1 km and source depth is 12 m. A 16 hydrophone VLA is used as a receiver where the first hydrophone is at 6 m and the interspacing between hydrophones is 4 m. Figure 4.4 (b) shows the corresponding beamformer output. These results were obtained from a simulated scenario which is explained further in section 4.5.1. Figure 4.4 (a) shows that each hydrophone of the array receives the same wavefront with different delays. Figure 4.4 (b) shows the beamforming results where different arrivals can be characterized based on the angle of arrival. The first two arrivals are the direct and top arrivals which arrive very closely at 6 and 8 degrees respectively. The next two wavefronts are the bottom reflected arrivals arriving at -13 and -15 degrees and the last two wavefronts are again from the surface, arriving at 18 and 21 degrees.

4.3 The beamformer-FSpTR approach

The basic idea of integrating BF and FSpTR is to apply the FSpTR operator for each angle of observation of the BF. Figure 4.5 shows the block diagram of the current implementation of the BF-FSpTR. For the purpose of clarification g_i and g'_i represent the channel IRs between the source and the VLA hydrophone, i , at different instants of time. In case of no channel variability $g_i \equiv g'_i$, and in the presence of channel variability there will be a mismatch between the initial IRs, g_i and the subsequent IRs g'_i . For the rest of the section g_i and g'_i will be termed as initial-field and mismatched-field respectively. The extension of BF-FSpTR to data communications will be explained in section 4.4.

It should be noted that the current BF-FSpTR system is implemented in the frequency domain, thus after the FFT operation of the channel IRs all the blocks operate in the frequency domain over the corresponding Frequency Response (FRs) up to the IFFT block.

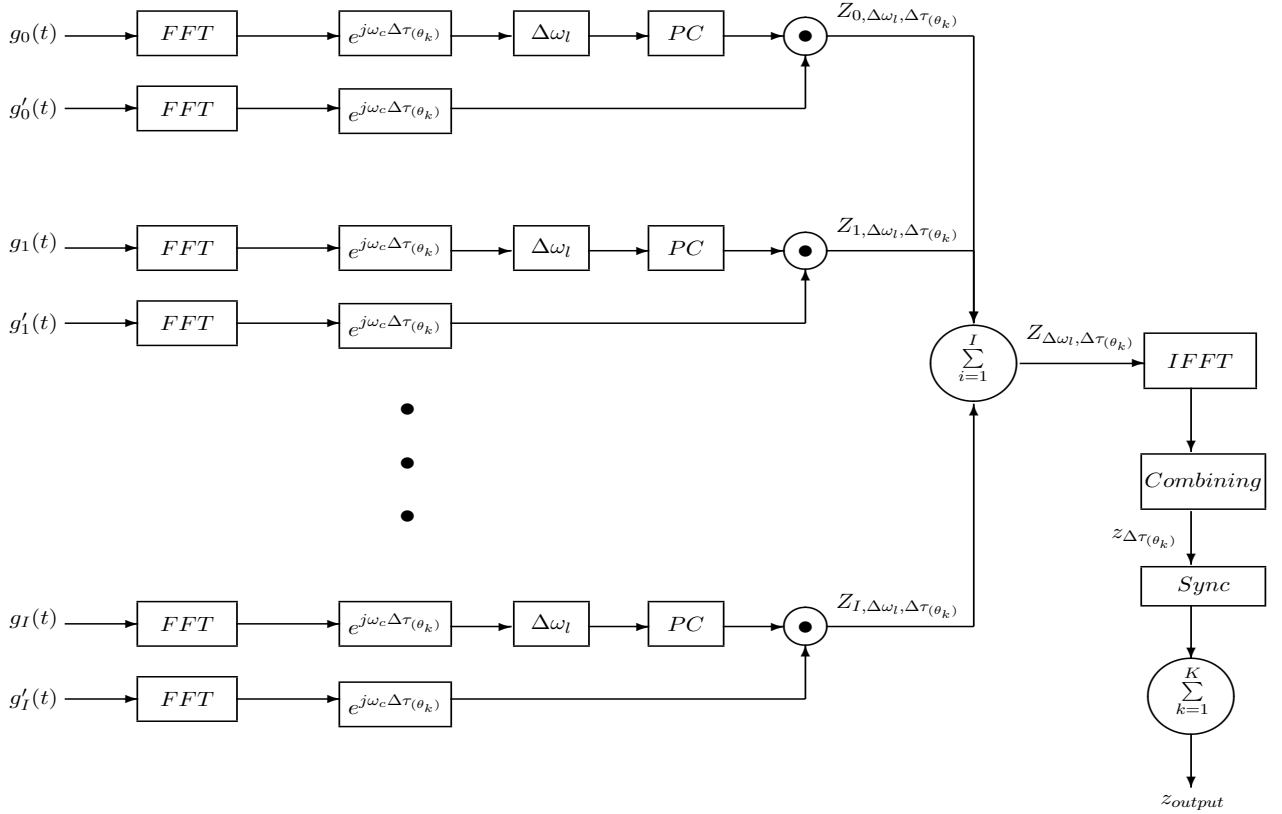


Figure 4.5: Block Diagram of the BF-FSpTR

The second block (which is the exponential block) performs the BF phase shift operation corresponding to each angle of observation, θ_k , for both initial and mismatched-field while the third block performs the FSpTR frequency shift operation over the initial field to compensate ("track") for the channel variability of g'_i . In the FSpTR frequency shift operation a set of l , frequency shifts are applied to all phase shifted versions of the initial field. The main purpose of applying the phase shift operation is to isolate (*i.e.* to give coherence to) different paths in the initial and mismatched field while the frequency shift operation provides the compensation for the mismatch between the initial and the mismatch field. Thus the output of the frequency shift block, $\Delta\omega_l$, becomes a "compensated-initial-field". The effective frequency shift compensation is only achieved after the combining block as the frequency shift

operation only applies a set of frequencies on the initial field and the selection of the optimal frequency shift is obtained after the combining block. The frequency shift block is followed by the Phase Conjugation (PC) and the multiplication block, which are the usual blocks of the pTR system. The PC block, being the counterpart of time reversal in time domain, performs the Time Reversal operation on the “compensated-initial-field” by taking the conjugate of the “compensated-initial-field”. The multiplication operation is equivalent to the convolution between the mismatch-field and the phase-conjugated “compensated-initial-field” in the time domain. The output of the multiplication block is summed over all the hydrophones to get $Z_{\Delta\omega_l, \Delta\tau(\theta_k)}$. This summation block serves dual purposes in the BF-FSpTR system. In the BF context the summing operation gives the observation of the wavefront in the θ_k direction while in the FSpTR context it corresponds to the time focusing of the resulting acoustic field for the $\Delta\omega_l$ frequency shift. The Combining block, as in the usual FSpTR operation, selects the frequency-shift, $\Delta\omega_l$, that results in higher output power of $z_{\Delta\omega_l, \Delta\tau(\theta_k)}$. Such operation is applied for each angle θ_k to get $z_{\Delta\tau(\theta_k)}$, that corresponds to the frequency shifts that best compensates for the channel mismatch.

$$z_{\Delta\tau(\theta_k)} = \begin{bmatrix} z_{\Delta\tau(\theta_0)} \\ z_{\Delta\tau(\theta_1)} \\ \vdots \\ z_{\Delta\tau(\theta_K)} \end{bmatrix} \quad (4.2)$$

The synchronization block is implemented to align the phase of all the data signals corresponding to each angle of observation, which will be discussed in section 4.4. The output of the synchronization block is summed up over all angles to get the output of the BF-FSpTR system.

Figures 4.6 to 4.8 illustrate the behavior of the BF-FSpTR. In these three different simulated scenarios (further described in section 4.5.1), (a) represents the output IR observed

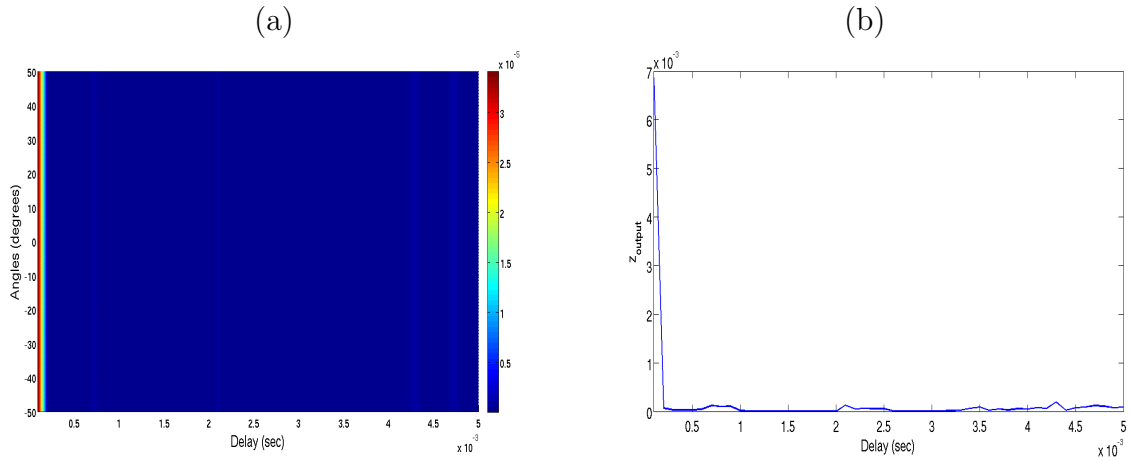


Figure 4.6: (a) Output of the combining block in figure 4.5 considering no frequency shift and identical IRs: (a) angle delay-spread plane, (b) sum over the angles, z_{output}

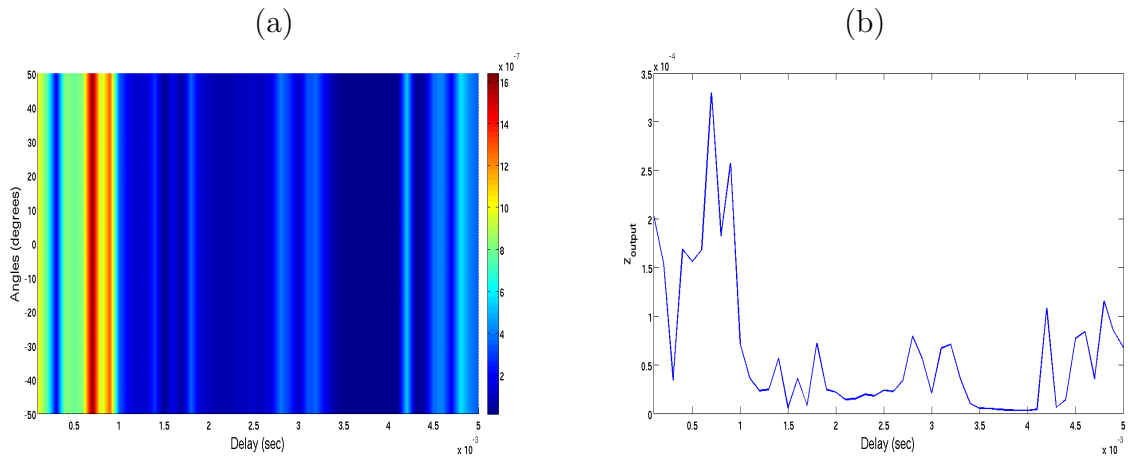


Figure 4.7: (a) Output of the combining block in figure 4.5 with no frequency shift and using mismatched IRs: (a) angle delay-spread plane, (b) sum over the angles, z_{output}

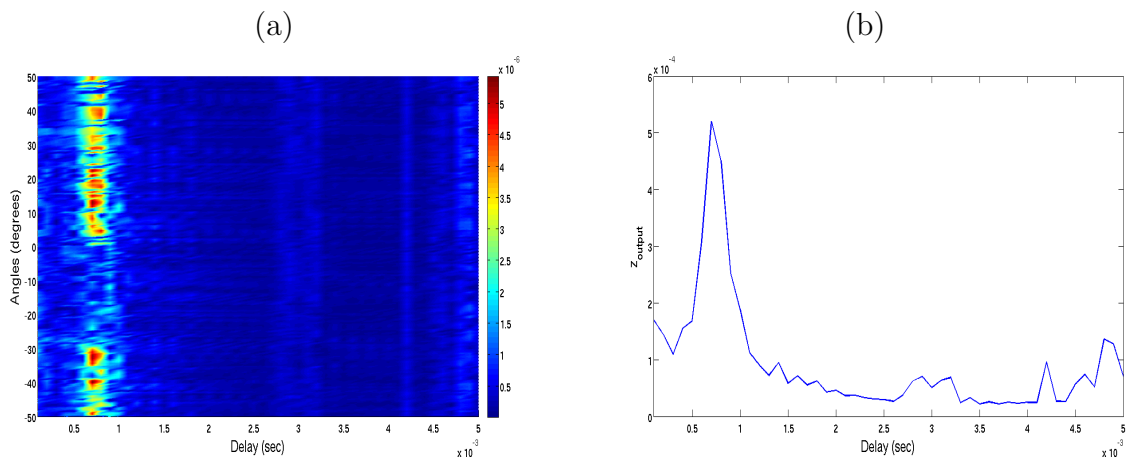


Figure 4.8: (a) Output of the combining block in figure 4.5 with optimal frequency shift compensation and using mismatched IRs: (a) angle delay-spread plane, (b) sum over the angles, z_{output}

for each angle, $z_{\Delta\tau(\theta_k)}$, and (b) shows the output after the summation over all angles, z_{output} . In all cases the initial-field, g_i , is the one shown in figure 4.4 (a). In case (i), depicted in figure 4.6, there is no mismatch and $g_i \equiv g'_i$; in case (ii), shown in figure 4.7, there is a mismatch between the initial-field and the mismatch-field, thus $g_i \neq g'_i$ but the combining block does not compensate for the channel mismatch and selects 0 Hz as the frequency shift. In figure 4.8, the same initial-field and the mismatch-field of case (ii) are being used, but now the combining block selects the optimal frequency, $\Delta\omega_l$, for each angle θ_k , depending on the maximum output power.

Figure 4.6 (a) shows that the field is almost constant for all angles with a single arrival at lag zero, which means that there is a focus in time and space. Figure 4.6 (b) shows that, after the summation over all angles, the overall IR becomes a Dirac impulse. Figure 4.7 shows that, the mismatch between the initial-field and the mismatch-field is not compensated by applying the frequency shift, thus there are multiple arrivals with different delays. Figure 4.7 (b) shows an overall IR with a strong multipath and a main arrival at 0.7 sec. Figure 4.8 (a) shows that when the frequency shift attempts to compensate for the channel mismatch there is a strong concentration of energy around 0.7 sec but it is not uniform over all angles. Figure 4.8 (b) reveals that this frequency compensation results in a strong multipath reduction and that the BF-FSpTR provides a partial compensation for the channel mismatch.

For underwater communication applications, the overall IRs observed in Figures 4.6 to 4.8 reveal that the Inter-Symbolic Interference (ISI) would be almost zero when there is no mismatch between g_i and g'_i while in case of channel mismatch, the ISI would be quite large. Finally, due to the frequency shift compensation there is a strong reduction in ISI, when compared with the mismatch.

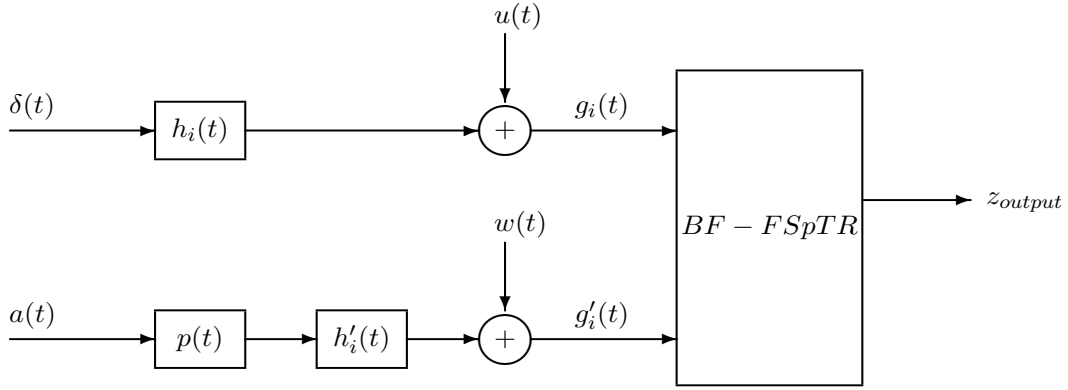


Figure 4.9: block diagram of the BF-FSpTR system, applied to underwater communications

4.4 The Beamformer-FSpTR communication system

Figure 4.9 shows the block diagram of the BF-FSpTR system when applied to underwater communications. The implementation of BF-FSpTR was explained in the last section where it was considered that g_i and g'_i were the channel IRs at different time instants. For the purpose of applying the BF-FSpTR for data communications g'_i should contain the information data sequence and g_i the channel IR estimates.

The proposed block diagram is shown in figure 4.9, where conceptually in the upper part of the diagram, the transmitted pulse $\delta(t)$ is passed through the channel $h_i(t)$ that represent the channel IRs during probe transmission, at hydrophone i of the VLA, further added with additive white Gaussian noise (AWGN), $u(t)$, resulting that $g_i(t) = h_i(t) + u_i(t)$. In the lower part of the block diagram the data signal $a(n)$ is pulse shaped by a root raised cosine signal and convolved with the channel IRs, h'_i , that represents the channel during the signal transmission. The noise $w(t)$ is added to the resulting signal to get $g'_i(t)$ and then fed to the

BF-FSpTR block. In order to apply the FSpTR frequency shift compensation, the channel IRs are assumed to be almost constant (frozen) during 0.25 second and g'_i is divided in slot of 0.25 second before being applied to the BF-FSpTR block [48].

The output of the BF-FSpTR block, z_{output} , will be the data, a_n , convolved with an overall IR similar to the one shown in figure 4.8 (b), as discussed in section 4.3. Similarly z_{output} is also divided in slots of 0.25 second duration and the frequency shift channel-variability compensation, provided by the FSpTR, is not applied to the instantaneous channel but to the channel-variability during the correspondent 0.25 second, which is assumed to be negligible.

An important implementation issue of this system is the synchronization of different phase shifted data signals, $z_{\Delta\tau(\theta_k)}$, which is done after the combining block, as shown in figure 4.9.

Different frequency shifts are applied to each signal, corresponding to each angle of observation of the beamformer, so when these signals are added the desired MSE gain is not achieved. In order to solve this problem, for this work, each data signal is synchronized with a known M-sequence which is transmitted every one second in the transmitted data signal.

The angular range of the beamformer is another parameter which affects the performance of the BF-FSpTR. The angular range is the set of angles used in the beamformer to search for different wavefronts. Figure 4.4 (b) shows that if an angular range of -10 to 10 degrees is used only two wavefronts would be compensated, and if a -50 to 50 degrees is used all 6 wavefronts would be considered.

The angular range of the system must be such that it incorporates all the arrivals reaching the receiver. Nevertheless the BF-FSpTR results have shown that even a smaller range of angles gives better performance than FSpTR as it compensates for each arrival separately.

4.5 Performance Comparison of FSpTR and BF-FSpTR

This section elaborates the performance comparison of the proposed system with the simple FSpTR system. In order to show the effectiveness of BF-FSpTR, simulated as well as real data results are presented in this section. In the first part of this section two simulated scenarios are presented in which the performance of BF-FSpTR is compared with FSpTR. The geometry of the simulated scenario is similar to the geometry of the real scenario presented in chapter 3. In the last part of this section real data results are shown. The real data set presented in this section is the same as presented in chapter 2 to show the performance of FSpTR in case of source depth variation.

4.5.1 Simulated Data Scenarios

In order to simulate the underwater environment, the Time Variable Acoustic Propagation Model (TV-APM) was used, which was proposed in [17]. Two cases will be considered with a source-receiver range of 1 km and a source depth of 12 m. A 16 hydrophones VLA is considered with the first hydrophone placed at 6 m depth and an inter spacing between the hydrophones of 4 m. A flat surface is considered in TV-APM for both cases. This geometry

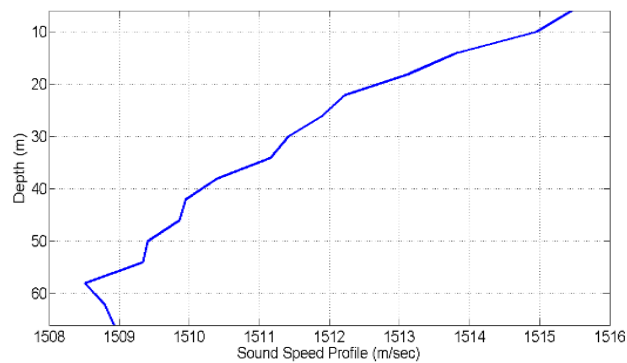


Figure 4.10: downward refracting sound speed profile.

is similar to the real environment presented in chapter 3. Figure 4.10 shows the sound speed profile (SSP) used in TV-APM for both cases, which is the same as in chapter 3.

In the first case the source is considered to be moving only along the vertical direction with the velocity of 0.5 m/s. Figure 4.4 (a) shows the arriving pattern of the channel. It can be seen that there are six wavefronts arriving at the VLA. Figure 4.4 (a) also shows that the first wavefront is not exactly a single wavefront instead it is a combination of the direct arrival and the surface reflected arrival. Figure 4.4 (b) shows the beamformer result where all six wavefronts can be seen in the angle delay-spread plane. The negative angles shows the wavefronts from the bottom while the positive angles shows the wavefronts from the surface.

Figure 4.4 completely characterizes all the wavefronts. Figure 4.4 (a) shows that the initial wavefronts are the top arrivals as they have negative slope while the third and the fourth wavefronts are the bottom arrivals as they have positive slope. These observations are confirmed by figure 4.4 (b) where it can be seen that the initial wavefronts have positive angle

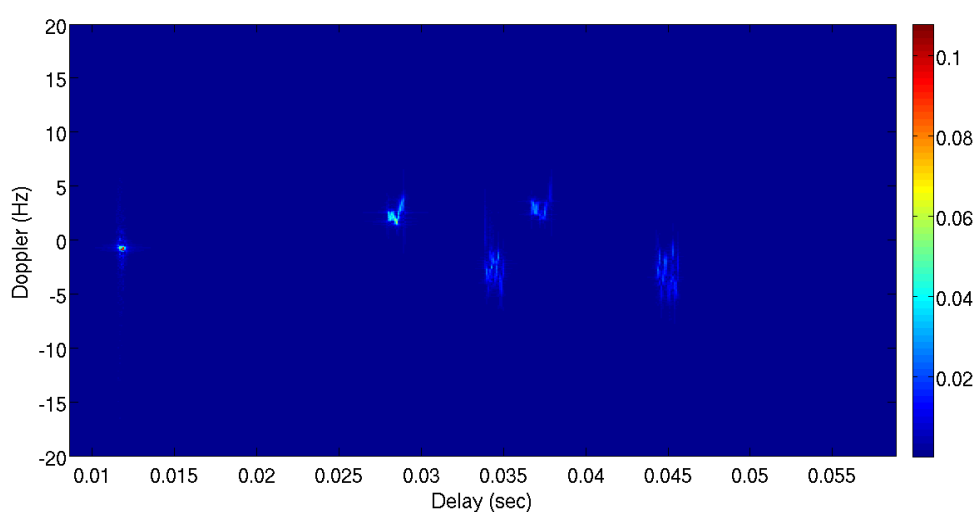


Figure 4.11: Doppler spread, at hydrophone 6 placed at 26 m depth, due to a source vertical motion of 0.5 m/s.

while the third and the fourth wavefronts have negative angle of arrival.

Figure 4.11 shows the Doppler spectrum of the channel at hydrophone 6 which is placed at 26 m depth. The source is moving only in the vertical direction so the values of Doppler for all wavefronts are very small. The Doppler value of the first wavefront which is considered to be the direct arrival is approximately -1 Hz. This small value of Doppler can be explained using equation (3.8) which shows that the Doppler value is related with the inner product of the relative velocities of the source and the receiver. As the source is moving in the vertical direction the inner product gives a very small value resulting in a small Doppler value.

As discussed in chapter 3 all the arrivals are affected by environmental variations in different ways thus each arrival have different values of Doppler. Such behavior can be clearly seen in figure 4.11 where the source motion in the vertical direction generates a small Doppler for the first two arrivals and a strong Doppler for the latter arrivals.

The second case also has the same geometry but now the source is considered to be moving in both horizontal and vertical direction with a velocity of 0.5 m/s each. The main purpose

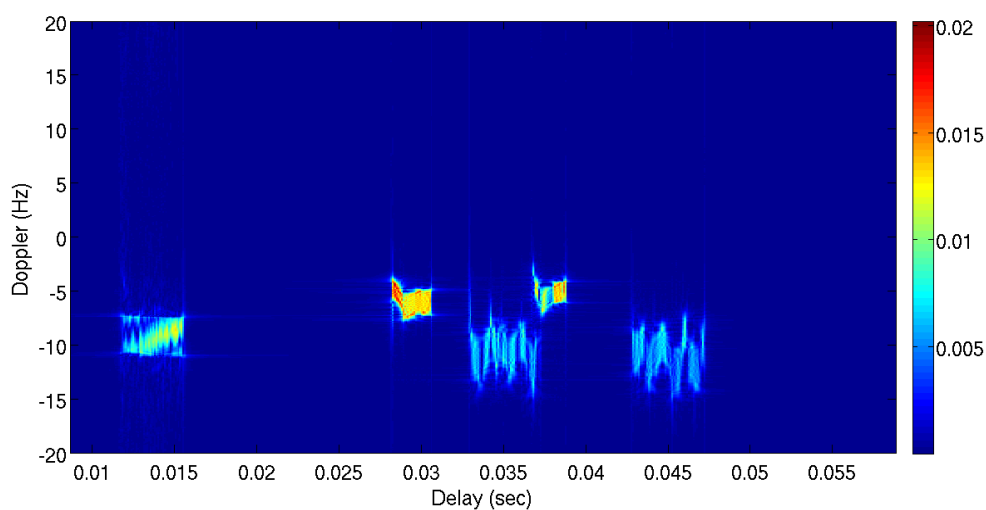


Figure 4.12: Doppler spread, at hydrophone 6 placed at 26 m depth, due to a source vertical and horizontal motion of 0.5 m/s each

of selecting this scenario is to study the performance of the BF-FSpTR system in a more challenging case. The initial arriving pattern of the channel and the corresponding beamformer are the same as for the first case which is shown in figure 4.4. Figure 4.12 shows the Doppler spectrum at hydrophone 6 which is placed at 26 m depth for the second case. Due to the simultaneous movement along horizontal and vertical directions, higher values of Doppler are induced in all arrivals.

4.5.2 Simulated Data Results

This subsection elaborates the performance comparison of FSpTR and BF-FSpTR in terms of MSE. The data set used for the analysis has a bit rate of 2000 bits/sec, sampling frequency of 2000 Hz and BPSK as the modulation scheme.

Figure 4.13 shows the performance comparison of BF-FSpTR and FSpTR in terms of MSE for the first case when the BF-FSpTR angular range of the beamformer is -10 to +10 degrees. In order to make the comparison between FSpTR and BF-FSpTR in similar conditions, only the initial two arrivals were used as IR estimate for the computation of FSpTR, since only these arrivals reach the receiver between -10 to 10 degrees (see figure 4.4). Figure 4.13 shows that the performance of BF-FSpTR is better than FSpTR during the whole 9 sec and gives a mean gain of 2.2 dB in terms of MSE. From the Doppler spectrum, shown in figure 4.11, it can be seen that each arrival is affected differently by the environmental variation and induces different Doppler in each arrival so a single frequency shift can not compensate for all these Doppler effects. This explains the superior performance of the BF-FSpTR over FSpTR since the considered two wavefronts are compensated with different frequency shifts

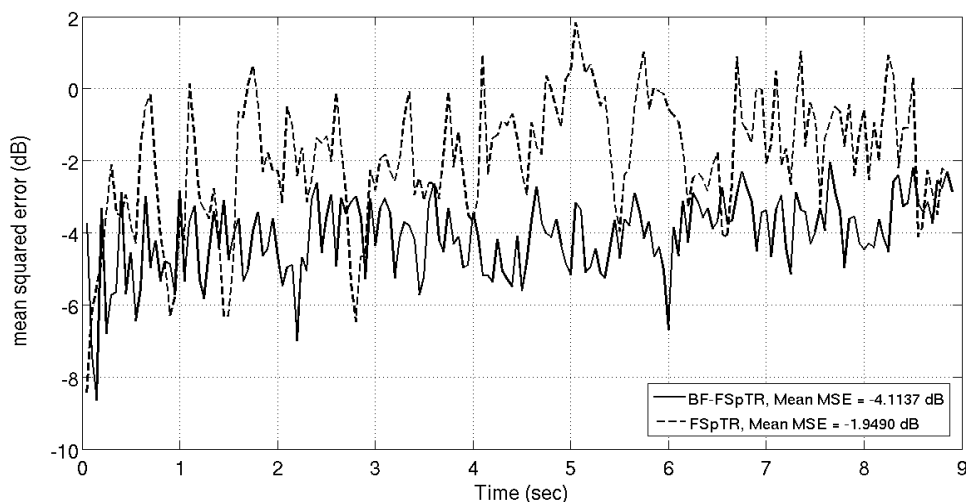


Figure 4.13: case (i) MSE performance of FSpTR and BF-FSpTR with a beamformer angular range of of -10 to +10 degrees.

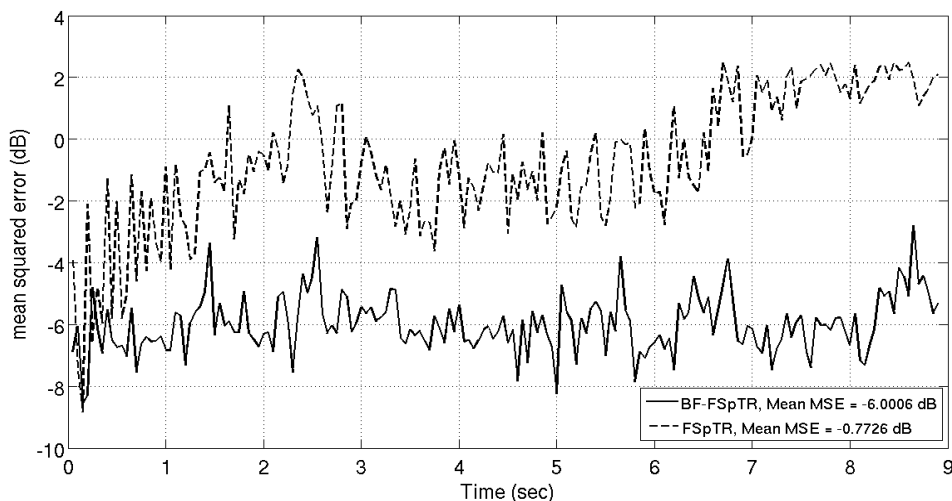


Figure 4.14: case (i) MSE performance of FSpTR and BF-FSpTR with a beamformer angular range of of -50 to +50 degrees.

by the BF-FSpTR.

Figure 4.14 shows the results of the same case but with the angular range of the BF-FSpTR increased to -50 to +50 degrees and all six wavefronts considered in the FSpTR IRs window. The performance of FSpTR degrades with time in this case, and the mean MSE value 0.77 dB is achieved for the whole 9 sec, while the performance of BF-FSpTR remains almost the same for the whole 9 sec with the mean MSE value of -6 dB. The main reason for

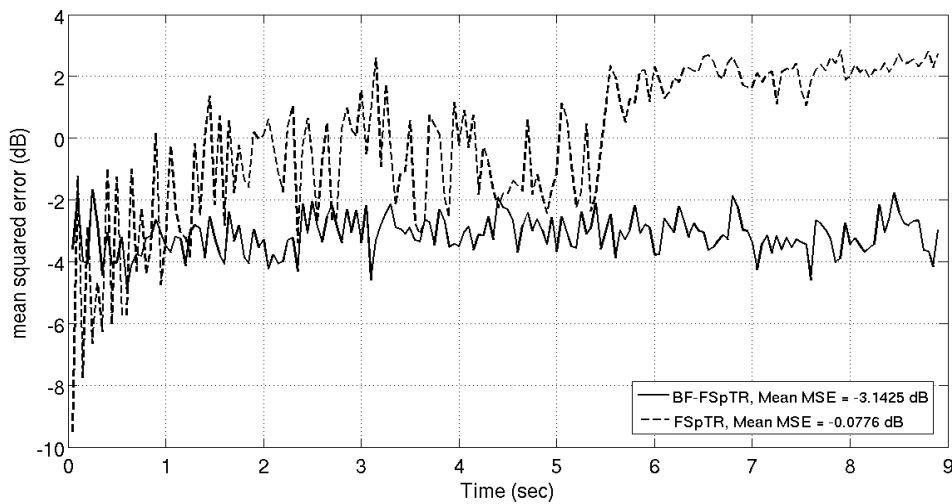


Figure 4.15: case (ii) MSE performance of FSpTR and BF-FSpTR with a beamformer angular range of of -50 to +50 degrees.

the FSpTR performance degradation is the fact that due to the increase in the number of arrivals a single frequency shift failed to compensate for all of them and thus the performance of FSpTR degrades. In the opposite side the BF-FSpTR compensates all the arrivals with different frequency shifts and thus the performance remains constant. Comparing figure 4.13 and figure 4.14 it can be observed that by increasing the angular range the BF-FSpTR mean gain in MSE increases 2 dB.

Figure 4.15 shows the MSE performance comparison for the second case between BF-FSpTR and FSpTR, for the angular range of -50 to 50 degrees. It can be seen that BF-FSpTR gives a mean MSE gain of 3.06 dB. Comparing figure 4.14 and figure 4.15 it can be seen that the performance of FSpTR is almost similar in both the simulated scenarios but the performance of BF-FSpTR degrades 2.8 dB in the second case. Figure 4.15 also shows that during the first second the FSpTR performance is better than the BF-FSpTR and that the BF-FSpTR remains almost constant during the all data set. The reason for this abnormal behavior is not completely clear and will be considered in future work.

4.5.3 Real data scenario

The data set shown in this section is the same as presented in chapter 2, section 2.3. This data set was collected during the UAB'07 experiment. During the experiment the source was suspended by a crane from a fixed platform, 10 m from shore, at an initial depth of 5 m. The receiver was a vertical array with 16 hydrophones uniformly spaced at 4 m between 6 m to 66 m depth. The communication range was approximately 1 km with the water column depth of 12 m at source location and about 120 m at array location. Figure 4.16 shows the zoomed version of the IR estimate shown in figure 2.4 (a) in chapter 2, to show only the wavefronts used in BF-FSpTR. It can be seen clearly that there are a large number of arrivals reaching the receiver. Figure 4.17 shows the angle of arrival of different wavefronts. It can be seen that there are two strong arrivals at approximately 3 degree and the third and fourth arrival at approximately 0 degree. Also there is another arrival at approximately -30 degree.

In the arriving pattern, shown in figure 4.16 the later arrivals are very unstructured and it

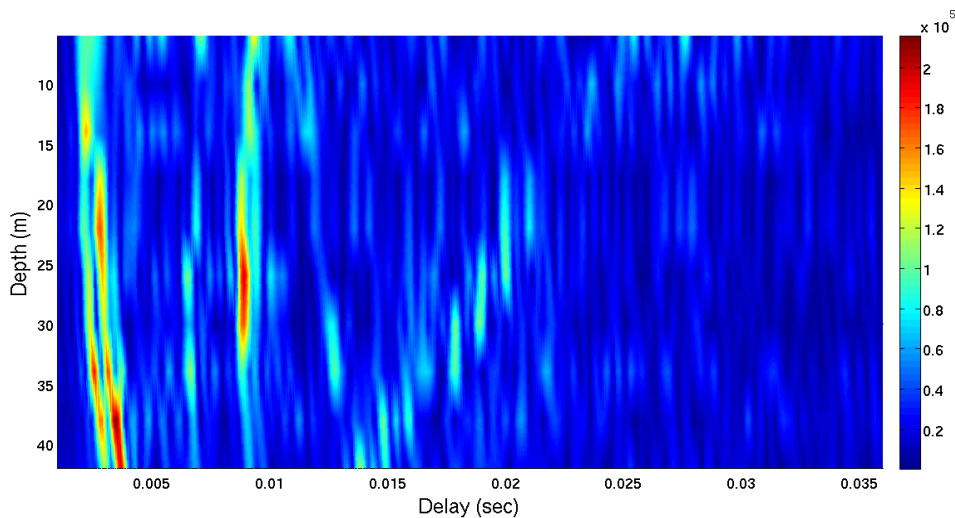


Figure 4.16: channel IR estimates of the real dataset.

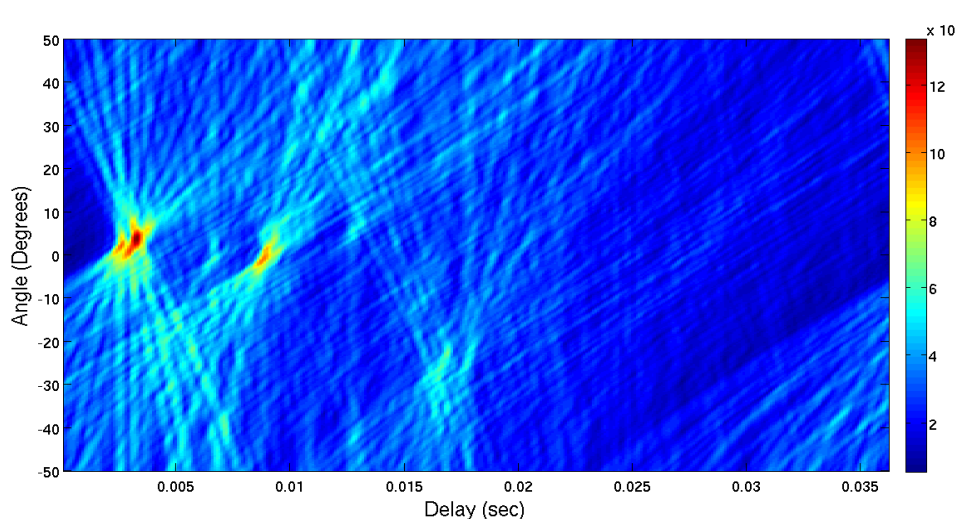


Figure 4.17: The Beamforming result showing the angle of arrival of different arrivals

is very difficult to differentiate between different wavefronts but the beamforming results in figure 4.17 differentiate between these wavefronts. In the arriving pattern, there is an arrival at approximately 0.01 sec (the one at 0°) which is almost vertical which means that it arrives at all hydrophone at the same time. This is an abnormal behavior for a later arrival as these arrivals are usually bottom or surface reflected and they reach all the hydrophones of the array with different delays. The probable reason for this behavior is that there may be a tilt in the hydrophone array due to the currents and thus all the hydrophones received the wavefront at almost the same time.

4.5.4 Real Data Results

The transmitted signal, presented in this section, comprises of 50 chirp signals followed by a data set of 100 seconds. The chirp transmission was used for the channel IR estimation and to study the channel variability and Doppler spread. Each chirp has a bandwidth of 2.5 kHz ranging from 5 to 7.5 kHz with 0.1 sec duration whereas data bandwidth ranges from

5.5 to 7 kHz with PSK-2 modulation and baud rate of 1000 bits/sec. A carrier frequency of 6250 Hz was used. During the transmission there are two controlled depth shifts from 4 to 4.5 m and 4.5 to 5 m at 12 and 42 sec respectively.

Figure 4.18 shows the performance of BF-FSpTR for an angular range of -10 to +10 degrees. Comparing the performance of FSpTR and BF-FSpTR in figure 4.18 it can be seen that BF-FSpTR outperforms FSpTR and there is a mean MSE gain of 2.3 dB. Another thing to be

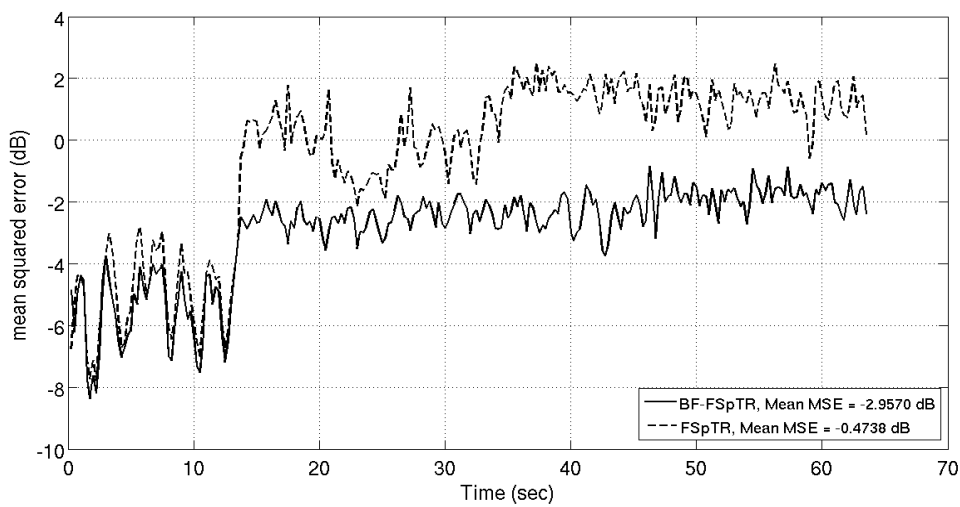


Figure 4.18: real data MSE performance comparison between FSpTR and BF-FSpTR with a beamformer angular range of of -10 to +10 degrees

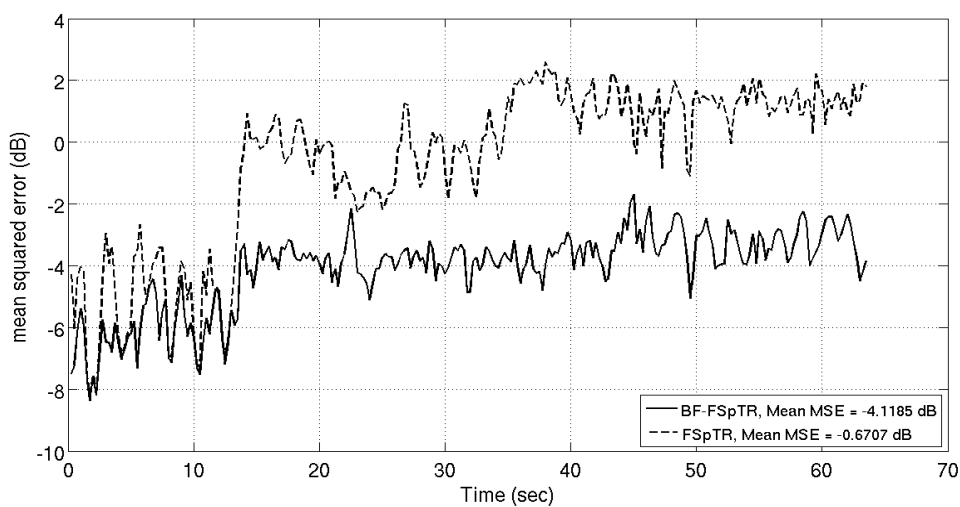


Figure 4.19: real data MSE performance comparison between FSpTR and BF-FSpTR with a beamformer angular range of of -50 to +50 degrees

observed in this figure is that BF-FSpTR performance degrades only in the first depth shift at 12 sec and then the performance remains almost constant. Comparing the performance of FSpTR in figure 4.18 and figure 2.9 in chapter 2, it can be seen that the performance of the FSpTR degrades in this case. The difference between the two cases is the size of the IR window. In chapter 2 the optimal performance of the FSpTR was presented by checking the MSE performance for different IR windows and the best performance was obtained for a small window containing only the initial two arrivals. In this case the IR window is selected based on the angle range which is -10 to 10 degrees and it can be seen in figure 4.17 that there are four arrivals reaching the receiver in this range. Thus the performance of FSpTR degrades due to the increase in the number of arrivals.

Figure 4.19 shows the performance in the same scenario but the angular range is increased to -50 to +50 degrees and the improvement in the performance is clearly visible. The overall behavior of BF-FSpTR along time is almost the same as in figure 4.18 but now there is a mean gain in MSE of 3.5 dB. On the other hand the performance of FSpTR degrades by 0.2 dB which is due to the increase in the size of IR window which results in more arrivals and a single frequency shift fails to compensate for all arrivals. The effect of increasing the angular range can also be seen from the beamforming result in figure 4.17 where it is clearly visible that there are four arrivals between -10 to 10 degrees and there is another arrival at approximately -30 degrees. By increasing the angular range all the arrivals are included and compensated by the BF-FSpTR, thus improves the performance of the system.

4.6 Conclusion and Future Work

In this chapter a new signal processing technique called Beamformed FSpTR (BF-FSpTR) was presented. BF-FSpTR is an arrival-based approach which isolates different arrivals in the multipath environment and compensate for each arrival separately as each arrival is affected in a different way by the environmental variation, thus each arrival experiences different amount of Doppler. Based on these different values of Doppler, each arrival needs to be compensated separately. The performance comparison of BF-FSpTR approach with conventional FSpTR was presented. In this chapter BF-FSpTR was tested with two simulated data sets and one real data set collected during the UAB'07 experiment. Among the two simulated data sets the source was considered moving only in the vertical direction with a velocity of 0.5 m/s in the first case and in the second case the source was considered moving both in horizontal and vertical directions with a velocity of 0.5 m/s. The results showed that BF-FSpTR outperforms FSpTR. In the first case a mean gain of 5.3 dB was achieved in terms of MSE between FSpTR and BF-FSpTR, while in the second case a mean gain of 3.06 dB was achieved. In the real data set there were two controlled depth shifts of 0.5 m at 12 sec and 42 sec and BF-FSpTR compensated for both of these shifts and produced a mean gain of 3.5 dB in terms of MSE as compared to FSpTR. The effect of angular range of the beamformer was also studied in this work. It was observed that by increasing the angular range the performance of BF-FSpTR was improved which is due to the fact that by increasing the angular range, more arrivals are included and BF-FSpTR compensates for each of them separately by applying appropriate frequency shift resulting in higher gain in terms of MSE.

The work presented in this chapter includes some preliminary observations and results of the BF-FSpTR system. These results have shown that BF-FSpTR has the potential of improving the performance of the underwater communication system. BF-FSpTR is an open field of research so different issues should be addressed in future work to understand the behavior of the BF-FSpTR system in more detail.

Another important aspect of BF-FSpTR is the spatial focusing property of the BFpTR system. The idea of integrating beamformer in FSpTR system was motivated by the fact that the pTR systems lacks in exploiting the spatial focusing. By introducing the beamformer, this problem was addressed as shown in Figures 4.6 to 4.8 of section 4.3. On the other hand, the active time reversal system has the intrinsic property of exploiting the spatial focusing so there may be a relationship between the active time reversal system and the BF-FSpTR system which will be addressed in detail in the future work.

Chapter 5

Conclusions

In current underwater communication systems, the transmission link is established by acoustic waves, traveling from the source to the receiver through the underwater channel. These wireless underwater communication systems offer great challenges due to limited bandwidth availability and different time-variant perturbations of the underwater channel. Underwater acoustic communication systems are very sensitive to the environmental perturbations like source and receiver movements and surface variations and a small change in the source/receiver position greatly affects the performance of the underwater communication system.

In order to improve the performance of the underwater system it is necessary to study the properties of the underwater channel. The underwater channel is a double spread channel which spreads both in time and frequency. The spread in time is mainly due to the multipath structure of the channel as there are multiple wavefronts arriving at the receiver from different paths and each associated wavefront experience different delays. The spread in the frequency domain is due to the time variability of the channel. The main factors which make the underwater channel time-variable are the environmental variations like sound speed profile variations and surface motion. In order to improve the underwater acoustic communi-

cation systems it is necessary to make them account for these variations. This work addresses these problems and propose some methods to analyze and improve the performance of the underwater communication system.

This work is based on Passive Time Reversal (pTR). In pTR, a probe signal is transmitted ahead of the data signal to estimate the channel impulse response (IR). The estimated IR is then correlated, in a time reversed manner, with the data signal received at the receiver, resulting in temporal focusing of the received signal. This temporal focusing is greatly compromised in case of geometric variations, thus the performance of the system degrades rapidly. In order to solve this problem, a new version of pTR was proposed in [8], called Frequency Shift Passive Time Reversal (FSpTR) equalizer . The main idea of the FSpTR equalizer is to compensate for these geometric variations by applying a frequency shift in the estimated channel IR and then correlate it with the received data signal to get the output of the equalizer. The main difference between pTR and FSpTR is that in FSpTR the channel IR is frequency shifted and then correlated with the received signal while in pTR the channel IR is directly correlated with the received signal. In order to select the optimal frequency shift, a set of frequency shifts are applied to the IR and the optimal one is selected based on the maximum power of the output signal.

This FSpTR equalizer is applied on the real data of the UAB'07 experiment where some deliberate depth changes of 0.5 m are made at known instants of time. The results show that FSpTR successfully tracks these depth variations and compensates for these variations by using appropriate frequency shifts. Two data sets are presented in this work. In the first case, a depth change from 4 m to 4.5 m was made and in the second case two depth changes from 4 m to 4.5 m and 4.5 m to 5 m are tested. In both cases, the FSpTR outperformed

pTR and provided a gain of 1.2 dB and 0.8 dB respectively in terms of MSE.

In the real environment, the channel IR consists of multiple paths arriving from the transmitter to the receiver and each path is affected by different environmental variations. The current pTR communication system solve the problem of the time spread by providing the focusing in the time domain. FSpTR also tries to compensate for the time variability of the channel by applying a frequency shift in the IR but it fails to compensate completely as each path is affected by the environmental variations in a different way and a single frequency shift could not compensate for all these variations. The solution proposed for this problem is to compensate for each wavefront separately by selecting an appropriate frequency shift for each wavefront in accordance with the environmental effects experienced by it.

In the real environment, the multipath structure of the underwater channel is very complex and all the arrivals are merged into one another in time, which makes it difficult to differentiate between them. In order to study the effects of environmental variations on each arrival, a Doppler-based analysis method is proposed in this work, called Time Windowed Doppler Spectrum (TWDS). In the TWDS technique, the Doppler spectrum of the time windowed version of the IR is computed and based on the temporal variations in the Doppler spectrum, different arrivals are characterized in terms of geometry as direct, surface-reflected or bottom reflected arrivals.

The TWDS analysis showed that each wavefront is affected by the environmental variations in a different way, thus different values of Doppler are induced in each wavefront. In this work, real data from the CALCOMM'10 experiment is presented . The results show that the magnitude of the Doppler is a function of the path length from the transmitter to the receiver and the sign of the Doppler value is dictated by the compression or expansion in

the path length due to the environmental variations e.g. source/receiver motion and surface variations. In this work, the direct and surface reflected paths are studied in details. It is shown that due to surface wave motion, the surface reflected arrival is compressed and expanded in a periodic manner resulting in a wave like motion in the Doppler domain. Since the source was towed close to the surface during the experiment, the direct path also experienced the effects of surface variations in the form of wave-like Doppler variations.

In TWDS, the temporal windowing of the IR produces side lobes which compromise the resolution in the Doppler domain. A time frequency analysis technique, proposed in [49], is used to solve this problem. This technique uses a combination of Wigner Transform (WT) and Short Time Fourier Transform (STFT) to improve the resolution in the time-frequency plane.

An improved version of FSpTR, called Beamformed FSpTR (BF-FSpTR), is proposed in this work. BF-FSpTR is based on the observations of TWDS which suggest that each wavefront is affected by the environmental variations in a different manner thus different frequency shifts are required for each wavefront to compensate for these environmental variations. In order to separate each wavefront, the beamforming technique is used. The beamforming technique separates each wavefront based on the angle of arrival and these wavefronts are fed separately to the FSpTR equalizer. The FSpTR equalizer selects the optimum frequency shift for each wavefront, hence the proposed technique is called BF-FSpTR. BF-FSpTR improves the temporal focusing by compensating for the channel variability on each wavefront resulting in improving the performance of the system.

The effect of the angular range of the beamformer, on the performance of the system, is also discussed in this work. It is observed that increasing the angular range greatly improves the

performance of the system. The reason for this improvement is the fact that by increasing the angular range more arrivals from wider angles are incorporated and coherently combined resulting in higher output energy. The results of the BF-FSpTR clearly showed that it gives significant performance gain over the simple FSpTR. The BF-FSpTR system was tested with both simulated and real data. With simulated data two cases were considered. In the first case, the source was considered moving vertically with the velocity of 0.5 m/sec and in the second case the source was moving along both x and z direction with the velocity of 0.5 m/sec. In both cases the BF-FSpTR outperformed FSpTR and provided a gain of 5.3 dB and 3.06 dB respectively for an angular resolution of -50 to 50 degrees. In case of real data the same scenario of the UAB'07 experiment was presented where two depth shifts were made from 4 m to 4.5 m and 4.5 m to 5 m. The results show that BF-FSpTR compensated for both the depth shifts and provided a gain of 3.5 dB as compared to FSpTR for the same angular resolution.

The main goal of this work is to address various issues in multi-channel underwater communication and present some solutions for these systems to make them suitable for high data rate applications. An important issue which needs to be addressed in the future, is the computational complexity of the BF-FSpTR equalizer so that it can be implemented in hardware, like modems. This will enable us to commercialize the system and attain maximum benefit from it.

Bibliography

- [1] O. Hinton, G. Howe, and A. Adams. An adaptive high bit rate sub-sea communications system. *Proceeding of European Conference on Underwater Acoustics, Bressels, Belgium*, pages 75–79, 1992.
- [2] M. Suzuki, and T. Sasaki. Digital acoustic image transmission system for deep sea research submersible. *Proceeding of Oceans '92, Newport, RI*, pages 567–570, 1992.
- [3] J. Fischer, K. Bennet S. Reible J. Cafarella and I. Yao. A high rate underwater acoustic data communication transceiver. *Proceeding of Oceans '92, Newport, RI*, pages 571–576, 1992.
- [4] G. Sandsmark, A. Torsvik and J. Hovem. Shallow water coherent acoustic data transmission. *Proceeding of European Conference on Underwater Acoustics, Bressels, Belgium*, pages 88–91, 1992.
- [5] A. Silva, J. Gomes, S. M. Jesus and V. Barroso. Underwater acoustic communication using a time-reversal mirror approach. *5th European Conference on Underwater Acoustics*, July 2000.
- [6] G. F. Edelmann, T. Akal, W. S. Hodgkiss, S. Kim, W. A. Kuperman, and H. C. Song. An initial demonstration of underwater acoustic communication using time reversal.

- IEEE J. Oceanic Eng.*, 27:602–609, 2002.
- [7] M. Heinemann, A. Larraza, K. B. Smith,. Experimental studies of applications of time-reversal acoustics to noncoherent underwater communications. *J. Acoust. Soc. Am.*, 113:3111–3116, 2003.
- [8] António João Silva. Environment based underwater communications. *PHD Dissertation University of Algarve*, 2009.
- [9] C.L. Pekeris. Theory of propagation of explosive sound in shallow water. *Geological Society of America Memoir*, 27:1–117, 1948.
- [10] Perkins J. S Kuperman W. A, Porter M. B. and Piacsek A. A. Rapid three dimensional ocean acoustic modelling of complex environments. In *12th IMACS world Congress on Scientific Computation*, R. Vichnevetsky, P. Borne and J. Vignes Eds 2, pages 231–233, 1988.
- [11] M.J. Buckingham. Ocean-acoustic propagation models. *J. Acoustique*, Juin:223–287, 1992.
- [12] Finn B. Jensen, William A. Kuperman, Micheal B. Porter and Henrik Schmidt. *Computational Ocean Acoustics*. American Inst. of Physics, 2000.
- [13] Tolstoy I. and Clay C. S. *Ocean Acoustics: Theory and Experiment in Underwater Sound*. McGraw-Hill, New York, 1966.
- [14] James C. Preisig. Performance analysis of adaptive equalization for coherent acoustic communications in the time-varying ocean environment. *The Journal of the Acoustical Society of America*, 118(1):263–278, 2005.

-
- [15] R.H. Owen, B.V. Smith, and R.F.W. Coates. An experimental study of rough surface scattering and its effects on communication coherence. In *OCEANS '94. 'Oceans Engineering for Today's Technology and Tomorrow's Preservation.'* Proceedings, volume 3, pages III/483 –III/488 vol.3, sep 1994.
- [16] A. Essebbar, G. Loubet, and F. Vial. Underwater acoustic channel simulations for communication. In *OCEANS '94. 'Oceans Engineering for Today's Technology and Tomorrow's Preservation.'* Proceedings, volume 3, pages III/495 –III/500 vol.3, sep 1994.
- [17] A. Silva, O. Rodriguez, F. Zabel, J. Huilery, and S. M. Jesus. Underwater acoustics simulations with time variable acoustics propagation model. *Proceeding of 10th European Conference on Underwater Acoustics*, 2:989–996, July. 2010.
- [18] S. M. Flatte. Sound transmission through a fluctuating ocean. *Journal of Sound and Vibration*, 70, Issue 4:611–612, 1979.
- [19] D. Rouseff, D.R. Jackson, W.L.J. Fox, C.D. Jones, J.A. Ritcey, and D.R. Dowling. Underwater acoustic communication by passive-phase conjugation: theory and experimental results. *Oceanic Engineering, IEEE Journal of*, 26(4):821 –831, oct 2001.
- [20] Stojanovic M. Low complexity ofdm detector for underwater acoustic channels. In *OCEANS 2006 MTS/IEEE Conference and Exhibition, Boston, MA, USA*, pages 1–6, Sept. 2006.

-
- [21] Gomes J.; Silva A.; Jesus S.;. Ofdm demodulation in underwater time-reversed shortened channels. In *OCEANS 2008 MTS/IEEE Conference and Exhibition, Quebec City, Canada*, pages 1–8, Sept. 2008.
- [22] D. Kilfoyle, and A. Baggeroer. The state of art in underwater acoustics telemetry. *IEEE J. Ocean. Eng.*, 25, no. 1:4–27, Jan. 2000.
- [23] M. Stojanovic, J. Catipovic and J. Proakis. Coherent communications over long range acoustic telemetry channels. *NATO ASI Series on Acoustic Signal Processing for Ocean Exploration*, pages 607–612, 1993.
- [24] J. Proakis. *Digital Communications*. McGraw-Hill, New York,, 1989.
- [25] M. Stojanovic, J. Catipovic, and J. G. Proakis. Adaptive multichannel combining and equalization for underwater acoustic communications. *J. Acoust. Soc. Am.*, 94:1621–1631, 1993.
- [26] M. Stojanovic, J. Catipovic, and J. G. Proakis. Reduced-complexity multi-channel processing of underwater acoustic communication signals. *J. Acoust. Soc. Am.*, 98:961–972, 1995.
- [27] Milica Stojanovic. Retrofocusing techniques for high rate acoustic communications. *The Journal of the Acoustical Society of America*, 117(3):1173–1185, 2005.
- [28] Gomes J.; and Barroso V.;. Asymmetric underwater acoustic communication using a time-reversal mirror. In *OCEANS 2000 MTS/IEEE Conference and Exhibition, Providence, RI, USA*, volume 3, pages 1847–1851, Sept. 2000.

-
- [29] W. A. Kuperman, William S. Hodgkiss, Hee Chun Song, T. Akal, C. Ferla, and Darrell R. Jackson. Phase conjugation in the ocean: Experimental demonstration of an acoustic time-reversal mirror. *The Journal of the Acoustical Society of America*, 103(1):25–40, 1998.
- [30] J. S. Kim, H. C. Song, and W. A. Kuperman. Adaptive time-reversal mirror. *The Journal of the Acoustical Society of America*, 109(5):1817–1825, 2001.
- [31] G.F. Edelmann, W.S. Hodgkiss, S. Kim, W.A. Kuperman, H.C. Song, and T. Akal. Underwater acoustic communication using time reversal. In *OCEANS, 2001. MTS/IEEE Conference and Exhibition*, volume 4, pages 2231 –2235 vol.4, 2001.
- [32] M. Stojanovic; L. Freitag; and M. Johnson. Channel-estimation-based adaptive equalization of underwater acoustic signals. In *OCEANS 1999 MTS/IEEE Conference and Exhibition, Seattle, USA*, pages 985–990, Sept. 1999.
- [33] Vilaipornsawai U.; Silva A.J.; Jesus S.M.;. Underwater communications for moving source using geometry-adapted time reversal and dfe: Uan10 data. In *OCEANS 2011 IEEE Conference, Santandar, Spain*, pages 1–7, June 2011.
- [34] Zoi-Heleni Michalopoulou. Matched-impulse-response processing for shallow-water localization and geoacoustic inversion. *The Journal of the Acoustical Society of America*, 108(5):2082–2090, 2000.
- [35] P. A. Bello. Characterization of randomly time-variant linear channels. *IEEE Transactions on Communications Systems.*, CS-11:360–393, Dec. 1963.

- [36] Ma X. and Michalopoulou Z. H. Matched arrival processing for efficient inversion in underwater acoustics. In *OCEANS 1999 MTS/IEEE Conference and Exhibition, Seattle, USA*, volume 3, pages 1577–1580, Sept. 1999.
- [37] Michalopoulou Z.H.; Ma X.; Picarelli M.; and Ghosh-Dastidar U.;. Fast matching methods for inversion with underwater sound. In *OCEANS 2000 MTS/IEEE Conference and Exhibition, Providence, RI, USA*, volume 1, pages 647–651, Sept. 2000.
- [38] W. Li and J. C. Preisig. Estimation of rapidly time-varying sparse channels. *Oceanic Engineering, IEEE Journal of*, 32(4):927 – 939, Oct. 2007.
- [39] Zamanizadeh E.; Gomes J.; Bioucas-Dias J.M.;. Identification and matching of sparse delay-doppler spread functions from high-frequency communications signals. In *OCEANS 2010 MTS/IEEE Conference and Exhibition, Seattle, USA*, pages 1–10, Sept. 2010.
- [40] Martin Siderius, and Michael B. Porter,. Modeling broadband ocean acoustic transmissions with time-varying sea surfaces. *J. Acoust. Soc. Am.*, 124:137–150, July 2008.
- [41] Nicolas F. Josso, Jerome I. Mars, Cornel Ioana, Cedric Gervaise, and Yann Stephan. On the consideration of motion effects in the computation of impulse response for underwater acoustics inversion. *J. Acoust. Soc. Am.*, 126:1739–1751, Oct. 2009.
- [42] J.A. Flynn, J.A. Ritcey, D. Rouseff, and W.L.J. Fox. Multichannel equalization by decision-directed passive phase conjugation: experimental results. *Oceanic Engineering, IEEE Journal of*, 29(3):824 – 836, july 2004.

- [43] Joao Gomes, Antonio Silva, and Sergio Jesus. Adaptive spatial combining for passive time-reversed communications. *The Journal of the Acoustical Society of America*, 124(2):1038–1053, 2008.
- [44] Chuprov. S. Interference structure of a sound field in a layered ocean. In *L. Brekhovskikh and I. Andreevoi, editors, Oceans Acoustics, Current state*, pages 71–91, Nuaka, Moscow. 1982.
- [45] A. Parvulescu and C. S Clay. Reproducibility of signal transmissions in the ocean. *Radio Electron Eng.*, 29:223–228, 1965.
- [46] Grachev. G. A. Theory of acoustic field invariants in layered waveguide. *Acoust. Phys.*, 39:33–35, 1993.
- [47] Hee Chun Song, W. A. Kuperman, and W. S. Hodgkiss. A time-reversal mirror with variable range focusing. *The Journal of the Acoustical Society of America*, 103(6):3234–3240, 1998.
- [48] A. Silva, S.M. Jesus, and J. Gomes. Environmental equalizer for underwater communications. In *OCEANS 2007*, pages 1 –7, 29 2007-oct. 4 2007.
- [49] Soo-Chang Pei, and Jian-Jiun Ding. Relations between gabor transforms and fractional fourier transforms and their applications for signal processing. *IEEE Transactions on Signal Processing.*, 55, no. 10:4839, Oct. 2007.
- [50] Michael B. Porter, and Y. C. Liu. Finite-element ray tracing, theoretical and computational acoustics. *World Scientific Publishing Co.*, 2, 1994.

-
- [51] Lawrence. J. Ziomek. *Fundamentals of Acoustic Field Theory and Space-Time Signal Processing*. CRC, Boca Raton. FL,, 1995.
- [52] A. Silva, F. Zabel, C. Martins,. Acoustic oceanographic buoy: a telemetry system that meets rapid environmental assessment requirements. *Sea Technology*, 47:15–20, Sept. 2006.
- [53] Leon. Cohen. *Time-Frequency Analysis*. Prentice Hall NJ, 1995.
- [54] H. L. Van Trees. *Optimum Array Processing: Part IV of Detection, Estimation, and Modulation*. John Wiley and Sons, New York, 2002.
- [55] J. Billingsley and R. Kinns. The acoustic telescope. *J. Sound Vib.*, 48:485–510, 1976.
- [56] L. R. LeBlanc and P. P Beaujean. Underwater communication in shallow water. *Oceanology 98, Brighton, UK*, 2:209–221, 1998.
- [57] L. LeBlanc. Angular-spectral decomposition beamforming for acoustic arrays. *Oceanic Engineering, IEEE Journal of*, 9(1):31 – 39, jan 1984.
- [58] Lester R. LeBlanc and John I. Salisbury. High resolution wavenumber-frequency methods for towed arrays. *The Journal of the Acoustical Society of America*, 90(6):3155–3160, 1991.
- [59] P.-P.J. Beaujean and L.R. LeBlanc. Spatio-temporal processing of coherent acoustic communications data in shallow water. In *OCEANS 2000 MTS/IEEE Conference and Exhibition*, volume 3, pages 1625 –1631 vol.3, 2000.